

Search for neutralino pair production at the CERN LHC

M. Demirci^{1,*} and A. I. Ahmadov^{2,†}

¹*Department of Physics, Karadeniz Technical University, 61080 Trabzon, Turkey*

²*Department of Theoretical Physics, Baku State University, Z. Khalilov Street 23, AZ-1148, Baku, Azerbaijan*

(Dated: March 17, 2014)

We provide the next-to-leading order (NLO) predictions for the neutralino pair production via quark-antiquark annihilation and gluon-gluon fusion at the CERN Large Hadron Collider, focusing on the lightest neutralino which is likely to be the lightest supersymmetric particle. The dependence of total LO, NLO cross sections, and K factor on the center-of-mass energy, the M_2 - μ mass plane, the squark mass, and the factorization and renormalization scales is comprehensively analyzed for three different scenarios in the minimal supersymmetric standard model and the constrained minimal supersymmetric standard model. We find that the LO cross section is considerably increased by the NLO correction, and the K factor value is clearly related to the Higgsino/gaugino mass parameters, the squark mass, and the factorization and renormalization scales.

PACS numbers: 11.30.Pb, 12.60.Jv, 14.80.Ly, 14.80.Nb

I. INTRODUCTION

Weak scale supersymmetry (SUSY) (see, e.g., [1–3]) naturally involves an elegant mechanism for stabilizing the gauge hierarchy with regard to the effects of radiative corrections and allows unification of gauge couplings. Under the conservation of R -parity^{*}, it also provides a candidate for the dark matter (DM) postulated to explain astrophysical observations [6]. In R -parity-conserving SUSY models, the supersymmetric particles (sparticles) can only be produced in pairs, and the lightest sparticle (LSP) is absolutely stable. Among all the supersymmetric models, the minimal supersymmetric standard model (MSSM) is one of the most well-motivated and well-studied extensions of the standard model. The MSSM predicts many such new particles as sleptons, squarks, gluinos, the light/heavy neutral scalar (CP-even) Higgs bosons h^0/H^0 , a pseudoscalar (CP-odd) Higgs boson A^0 , a couple of charged Higgs bosons H^\pm , four neutralinos $\tilde{\chi}_i^0$ and two charginos $\tilde{\chi}_j^\pm$. The neutralinos and charginos are the mass eigenstates formed from the superposition of the neutral or charged superpartners of the electroweak gauge bosons and Higgs doublets (the so-called gauginos and Higgsinos, respectively). The lightest neutralino $\tilde{\chi}_1^0$ is usually supposed to be a weakly interacting massive particle which is consistent with the observations of the DM candidate (see, e.g., [7, 8]) in the form of the LSP for a number of SUSY breaking models. Therefore, it has to emerge as the final particle of the decay chain of each sparticle. That is why, a detailed analysis of the lightest

neutralino is quite important to the phenomenological and theoretical viewpoints of SUSY.

The experimental searches of the supersymmetric particles turn out to be one of the primary tasks of the experimental program at hadron colliders, especially at the Large Hadron Collider (LHC), after the recent discovery of the Higgs-like boson with a mass about 126 GeV [9, 10] is consistent with the MSSM-predicted range for mass of the lightest scalar Higgs h^0 . Moreover, the discovery (or exclusion) of weak-scale SUSY is reckoned among the highest physics priorities for the future LHC, including its high luminosity upgrade. Up to now, a great number of SUSY searches at the LHC have only exhibited null results related to discovery of any supersymmetric particles. In spite of the negative results, SUSY retains strong arguments in its favour as mentioned before. These searches which chiefly focus on the production of the colored superpartners such as squarks and gluinos have been performed by the ATLAS and CMS collaborations. Consequently, new stronger limits on the masses of the first two generations squarks and gluinos have been produced depending on details of the assumed parameters. These limits for a data set of an integrated luminosity of around 20 fb⁻¹ having been collected in 8 TeV pp collisions at the LHC are given in the following. According to recent ATLAS results [11, 12], a gluino mass is excluded up to 1.1 – 1.3 TeV in a mSUGRA/constrained MSSM (CMSSM) scenario at high values of the universal scalar mass parameter m_0 and in the gluino simplified models. The first two generations squark masses up to 700 – 780 GeV are also excluded in the squark simplified models. In addition, gluinos and squarks of equal mass are excluded for masses below 1.7 TeV in mSUGRA/CMSSM models. According to recent CMS results [13], the squark masses below 750 GeV and gluino masses of up to 1.1 TeV are excluded in the case where the squarks (gluinos) decay to one jet (two jets) and the LSP. Owing to these stronger limits on the masses of the squarks and gluinos, the attention in the experimental

* mehmetdemirci@ktu.edu.tr

† ahmadovazar@yahoo.com

^{*} R -parity, which is a discrete and multiplicative symmetry, is defined by $P_R = (-1)^{2S+3(B-L)}$ where B , L and S denote the baryon number, lepton number, and spin of the particle, respectively [4, 5]. Thus, this quantity is equal to $P_R = +1$ for the particles of the Standard Model (including the Higgs bosons) and $P_R = -1$ for their superpartners.

researches of the supersymmetric particles starts to turn towards the electroweak production of the sleptons, neutralinos, and charginos.

On the other hand, naturalness suggests that masses of charginos, neutralinos and third generation sparticles should be a few hundreds of GeV range [14]. There are also searches for superpartners of gauge and Higgs bosons, but they depend significantly on their assumed compositions and decay modes [15]. The bound on the lightest neutralino mass is given by $m_{\tilde{\chi}_1^0} \gtrsim 46$ GeV at 95% CL, derived from the lower bound on chargino mass in the MSSM at the Large Electron Positron [16]. In the framework of the CMSSM including both sfermion and gaugino mass unification, this bound reaches to well above 100 GeV from the powerful constraints set by the recent LHC data [17].

Note that a detailed study of the production of the lightest neutralino $\tilde{\chi}_1^0$ and the next-to-lightest neutralino $\tilde{\chi}_2^0$ can provide significant information about the SUSY-breaking mechanism and the nature of the dark matter. Moreover, the pair production of neutralinos/charginos begins to come into question as a discovery channel of supersymmetry. Presently one of the gold-plated SUSY discovery channels is the production of $\tilde{\chi}_1^\pm \tilde{\chi}_2^0$ pairs decaying into trilepton final states. But, in case of higgsino LSP scenarios, for example appear in context of natural SUSY models, those trilepton searches loose efficiency and should be replaced by novel same-sign dilepton and 4-lepton searches [18].

It is known that the effect of higher-order contributions to cross section usually increases with increment of colliding energy and would be more significant at very high energies. For this reason, it is important to take into account one-loop contributions for neutralino pair production. In the present work we analyze the dependence of the neutralino pair production via the processes $pp(q\bar{q}) \rightarrow \tilde{\chi}_i^0 \tilde{\chi}_j^0$ at tree and one-loop levels, and $pp(gg) \rightarrow \tilde{\chi}_i^0 \tilde{\chi}_j^0$ at one-loop level on SUSY model parameters at the LHC energies, considering the allowed parameter region in the MSSM. There have been few papers dedicated to the investigations of these processes at one-loop level in literature as follows. Considering next-to-leading order (NLO) SUSY-QCD corrections, the direct production channels of charginos and neutralinos at the Tevatron and LHC, $p\bar{p}/pp \rightarrow \tilde{\chi}_i \tilde{\chi}_j + X$ have been worked in Ref. [19]. It has been inferred from Ref. [19] that the SUSY-QCD corrections are positive, increasing the mass range of corresponding particles that can be covered at these colliders by as much as percent 10. The neutralino pair production via gluon-gluon fusion in the framework of the mSUGRA has been investigated in Ref. [20], and this loop-mediated process has been concluded to be competitive with the quark-antiquark annihilation process. However, our results in present work have not exhibited this case depending on details of the SUSY model parameters. The neutralino pair production via quark-antiquark annihilation within MSSM for three different scenarios has been worked in Ref. [21]. The pair

production of neutralinos via quark-antiquark annihilation including the leading-log one loop radiative corrections and via gluon-gluon fusion at one-loop level (this process was computed with a numerical code) have been studied in Ref. [22]. The NLO SUSY-QCD corrections to the production of a pair of the lightest neutralinos in association with one jet in the framework of the phenomenological MSSM (p19MSSM) have been computed in Ref. [23]. Finally, recently in our previous paper (see Ref. [24]) we have also analyzed the leading and subleading electroweak (EW) corrections to the neutralino pair production at proton-proton collision, and we have found that the EW corrections supply sizeable contributions, in particular, for the process $pp \rightarrow \tilde{\chi}_2^0 \tilde{\chi}_2^0$.

Unlike the above-mentioned works, within the present work the most outstanding feature of our approach is the mechanism in selecting the input parameters. We recover the corresponding Lagrangian parameters as direct analytical expressions of appropriate physical masses without any restrictions on them in the MSSM. As a matter of fact, we mainly focus on the algebraically nontrivial inversion in order to obtain Higgsino and gaugino mass parameters. If we need to explicitly specify, we can say that using $\tan\beta$ and masses of charginos as input parameters, then we get the other ones being Higgsino/gaugino mass parameters, neutralino masses and mixing matrix.

The remainder of the present work proceeds in the following order: In Section II, the analytical results of the relevant amplitudes and cross sections are given for partonic process $q\bar{q} \rightarrow \tilde{\chi}_i^0 \tilde{\chi}_j^0$. In Section III, we give briefly information about one-loop contributions to neutralino pair production via quark-antiquark annihilation (in Subsection III A) and gluon-gluon fusion (in Subsection III B). In Section IV, we present definitions corresponding to our method and input parameters which are used in numerical calculations. In Section V, we give numerical results and discuss the corresponding SUSY parameters dependences of the cross section in detail for each scenario. Finally, the results appearing in Section V are summarized in Section VI.

II. THE LEADING-ORDER CALCULATION FOR THE NEUTRALINO PAIR PRODUCTION

In this section, after introducing the necessary couplings and Lagrangians in the MSSM, we serve up analytical results of amplitudes and cross section for the partonic process $q\bar{q} \rightarrow \tilde{\chi}_i^0 \tilde{\chi}_j^0$ at leading order (LO). The clean environment of proton-proton collision, together with the well-defined energy of the initial state, make this collision ideal for precision measurements of neutralinos properties. The associated production of neutralino pair via quark-antiquark collision at hadron colliders could be denoted by

$$q(p_1)\bar{q}(p_2) \rightarrow \tilde{\chi}_i^0(k_1)\tilde{\chi}_j^0(k_2), \quad (2.1)$$

where the labels in parentheses indicate the four momenta of the relevant particles. The cross section for subprocess (2.1) is parameterized in terms of the following Mandelstam variables,

$$\hat{s} = (p_1 + p_2)^2, \quad \hat{t} = (p_1 - k_1)^2, \quad \hat{u} = (p_1 - k_2)^2. \quad (2.2)$$

Introducing by (θ, p) scattering angle and momentum in the center-of-mass system of the final states neutralinos, for corresponding center-of-mass energy and momentums we have,

$$\begin{aligned} p &= \frac{1}{2\sqrt{\hat{s}}} \sqrt{(\hat{s} - m_{\tilde{\chi}_i^0}^2 - m_{\tilde{\chi}_j^0}^2)^2 - 4m_{\tilde{\chi}_i^0}^2 m_{\tilde{\chi}_j^0}^2}, \\ E_1 &= \frac{\hat{s} + m_{\tilde{\chi}_i^0}^2 - m_{\tilde{\chi}_j^0}^2}{2\sqrt{\hat{s}}}, \quad E_2 = \frac{\hat{s} + m_{\tilde{\chi}_j^0}^2 - m_{\tilde{\chi}_i^0}^2}{2\sqrt{\hat{s}}}, \\ p_1 &= \frac{\sqrt{\hat{s}}}{2}(1, 0, 0, 1), \quad p_2 = \frac{\sqrt{\hat{s}}}{2}(1, 0, 0, -1), \\ k_1 &= (E_1, p \sin \theta, 0, p \cos \theta), \\ k_2 &= (E_2, -p \sin \theta, 0, -p \cos \theta). \end{aligned} \quad (2.3)$$

In the following part, we give the corresponding couplings of the neutralino pair production in the MSSM. Using the standard notation, the Z^0 boson-neutralino-neutralino interactions are proportional to the following couplings:

$$\begin{aligned} O_{ij}^{\prime L} &= \frac{1}{2} [N_{i4} N_{j4}^* - N_{i3} N_{j3}^*], \\ O_{ij}^{\prime R} &= \frac{1}{2} [N_{i3}^* N_{j3} - N_{i4}^* N_{j4}], \end{aligned} \quad (2.4)$$

where $O_{ij}^{\prime R} = -O_{ij}^{\prime L*}$, and N denotes neutralino mixing matrix being a 4×4 unitary matrix which diagonalizes the neutralino mass matrix. Neglecting generational mixing in the squark sectors, then, the neutralino-quark-squark interactions are proportional to the relevant couplings,

$$\begin{aligned} C_{\tilde{\chi}_i^0 \tilde{q} k q}^L &= [(e_q - I_q^3) s_W N_{i1} + I_q^3 c_W N_{i2}] \delta_{kL} \\ &\quad + \frac{c_W m_q (N_{i4} \delta_{qu} + N_{i3} \delta_{qd})}{2m_W (\sin \beta \delta_{qu} + \cos \beta \delta_{qd})} \delta_{kR}, \\ C_{\tilde{\chi}_i^0 \tilde{q} k q}^R &= (-e_q s_W N_{i1}^*) \delta_{kR} \\ &\quad + \frac{m_q c_W (N_{i4}^* \delta_{qu} + N_{i3}^* \delta_{qd})}{2m_W (\sin \beta \delta_{qu} + \cos \beta \delta_{qd})} \delta_{kL}, \end{aligned} \quad (2.5)$$

and for the Z^0 boson-quark-quark couplings, we have

$$\begin{aligned} C_{Zqq}^L &= 2I_q^3 (1 - 2s_W^2 |e_q|), \\ C_{Zqq}^R &= -2s_W^2 e_q, \end{aligned} \quad (2.6)$$

where e_q and I_q^3 are the fractional electromagnetic charge and the third component of the weak isospin of quark q ; such that $I_{qL}^3 = \pm 1/2$ ($I_{qR}^3 = 0$) for left-handed (right-handed) up- and down-type quarks. The sine and cosine of the electroweak mixing angle θ_W are denoted by $c_W \equiv \cos \theta_W = m_Z / m_W$ and $s_W \equiv \sin \theta_W = \sqrt{1 - c_W^2}$.

In the above couplings, furthermore, q refers to up- and down-type quarks, while the label k refers to left- and right-handed for squark. Finally, δ_{kl} appearing in Eq. (2.5) is the kronecker delta function which is equal to 1 if the labels k, l are the same, and 0 otherwise; for instance $\delta_{qu} = 1$ for up-type quark ($q \equiv u$) and $\delta_{kL} = 0$ for right-handed squark ($k \equiv R$). We use it to display the neutralino couplings to both an up-type quark/squark and a down-type quark/squark in the same relation. The couplings of the neutralino to Z^0 boson and (s)quark are considerably dependent on the corresponding elements of the neutralino mixing matrix N_{ij} ($i, j = 1, \dots, 4$) as seen from the above couplings. Considering neutralino mass eigenstate basis, the neutralino interactions to corresponding particles in question are obtained from the following Lagrangians [2],

$$\mathcal{L}_{\tilde{\chi}_i^0 \tilde{q} k q} = -\frac{\sqrt{2}g}{c_W} \tilde{\chi}_i^0 q \left[C_{\tilde{\chi}_i^0 \tilde{q} k q}^{L*} P_L + C_{\tilde{\chi}_i^0 \tilde{q} k q}^{R*} P_R \right] \tilde{q}_k, \quad (2.7)$$

$$\mathcal{L}_{Z^0 \tilde{\chi}_i^0 \tilde{\chi}_j^0} = \frac{g}{c_W} Z_\mu \tilde{\chi}_i^0 \gamma^\mu \left[O_{ij}^{\prime L} P_L + O_{ij}^{\prime R} P_R \right] \tilde{\chi}_j^0, \quad (2.8)$$

$$\mathcal{L}_{Z^0 q \bar{q}} = -\frac{g}{2c_W} \bar{q} \gamma^\mu \left[C_{Zqq}^L P_L + C_{Zqq}^R P_R \right] q Z_\mu, \quad (2.9)$$

where q , \tilde{q}_k and $\tilde{\chi}_i^0$ are four-component spinor fields of the quark, squark and neutralino, respectively; $P_{R,L} = \frac{1}{2}(1 \pm \gamma^5)$ are the chiral projectors; and $g = e/s_W$ is the $SU(2)$ gauge coupling. Note that the Higgsino and gaugino components of the neutralino in the $Z \tilde{\chi}_i^0 \tilde{\chi}_j^0$ and $q \tilde{q}_k \tilde{\chi}_i^0$ coupling are controlled by the neutralino mixing matrix as shown in the above Lagrangians.

The Feynman diagrams of the partonic process $q\bar{q} \rightarrow \tilde{\chi}_i^0 \tilde{\chi}_j^0$ at leading level are displayed in Fig. 1. We neglect the contributions from the Feynman diagrams including the couplings $H^0/G^0/A^0 - q - q$ seeing that the strength of Yukawa coupling is proportional to the fermion mass and masses of the first two generations quarks are relatively small and could be ignored. Nevertheless, we will take into account these couplings and contributions of this vertex for bottom quark in a further work. Consequently, the subprocess for neutralino pair production contains an s -channel contribution through exchanging the Z^0 boson, t - and u -channel contributions via exchanging of the squarks as shown in Fig. 1. The leading-level contributions to the amplitude emerging from the three channels are given by

$$\begin{aligned} T_{\hat{s}} &= \frac{-g^2 D_Z(\hat{s})}{2c_W^2} \left[\bar{u}_i(k_1) \gamma_\mu (O_{ij}^{\prime L} P_L + O_{ij}^{\prime R} P_R) v_j(k_2) \right] \\ &\quad \cdot \left[\bar{v}(p_2) \gamma^\mu (C_{Zqq}^L P_L + C_{Zqq}^R P_R) u(p_1) \right], \end{aligned} \quad (2.10)$$

$$\begin{aligned} T_{\hat{t}} &= \sum_k \frac{2g^2}{(\hat{t} - m_{\tilde{q}_k}^2) c_W^2} \left[\bar{u}_i(k_1) (C_{\tilde{\chi}_i^0 \tilde{q}_k q}^L P_L + C_{\tilde{\chi}_i^0 \tilde{q}_k q}^R P_R) u(p_1) \right] \\ &\quad \cdot \left[\bar{v}(p_2) (C_{\tilde{\chi}_j^0 \tilde{q}_k q}^{R*} P_L + C_{\tilde{\chi}_j^0 \tilde{q}_k q}^{L*} P_R) v_j(k_2) \right], \end{aligned} \quad (2.11)$$

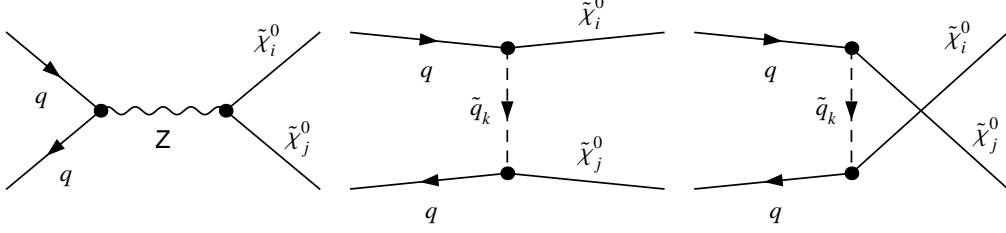


FIG. 1. Feynman diagrams of the partonic process $q\bar{q} \rightarrow \tilde{\chi}_i^0 \tilde{\chi}_j^0$ at leading level.

$$T_{\hat{u}} = \sum_l \frac{-2g^2}{(\hat{u} - m_{\tilde{q}_l}^2)c_W^2} \left[\bar{u}_j(k_2)(C_{\tilde{\chi}_j^0 \tilde{q}_l q}^L P_L + C_{\tilde{\chi}_j^0 \tilde{q}_l q}^R P_R)u(p_1) \right] \cdot \left[\bar{v}(p_2)(C_{\tilde{\chi}_i^0 \tilde{q}_l q}^{R*} P_L + C_{\tilde{\chi}_i^0 \tilde{q}_l q}^{L*} P_R)v_i(k_1) \right], \quad (2.12)$$

where the labels k, l represent the summation over the exchanged left/right-handed components of squarks in the same flavor, and the labels i, j represent the type of the neutralinos in the final state. From the above amplitudes along with couplings (2.4) and (2.5), explicitly we note that purely Higgsino production dominates in the contribution coming from the s -channel diagram, whereas the t - and u -channel contributions are dominated by purely gaugino production. After averaging over colors and spins of incoming particles, the parton-level differential cross section in the analytic form is given by the following formula,

$$\frac{d\hat{\sigma}(q\bar{q} \rightarrow \tilde{\chi}_i^0 \tilde{\chi}_j^0)}{d\hat{t}} = \frac{1}{16\pi\hat{s}^2} \frac{1}{12} \left(\frac{1}{2} \right)^{\delta_{ij}} (M_{\hat{s}\hat{s}} + M_{\hat{t}\hat{t}} + M_{\hat{u}\hat{u}} - 2M_{\hat{s}\hat{t}} + 2M_{\hat{s}\hat{u}} - 2M_{\hat{t}\hat{u}}), \quad (2.13)$$

where the factors $\frac{1}{12}$ is arising from spin and color averaging over the initial state and $(\frac{1}{2})^{\delta_{ij}}$ denotes the final identical particle factor. Using standard trace techniques, the squared amplitudes explicitly take the following form,

$$M_{\hat{s}\hat{s}} = \frac{g^4 |D_Z(\hat{s})|^2}{c_W^4} [(C_{Zqq}^L)^2 + (C_{Zqq}^R)^2] \left\{ O_{ij}^{\prime\prime L} O_{ij}^{\prime\prime L*} \times [(m_{\tilde{\chi}_i^0}^2 - \hat{u})(m_{\tilde{\chi}_j^0}^2 - \hat{u}) + (m_{\tilde{\chi}_i^0}^2 - \hat{t})(m_{\tilde{\chi}_j^0}^2 - \hat{t})] - [|O_{ij}^{\prime\prime L}|^2 + |O_{ij}^{\prime\prime R}|^2] m_{\tilde{\chi}_i^0} m_{\tilde{\chi}_j^0} \hat{s} \right\}, \quad (2.14)$$

$$M_{\hat{t}\hat{t}} = \sum_{k,l} \frac{4g^4}{(\hat{t} - m_{\tilde{q}_k}^2)(\hat{t} - m_{\tilde{q}_l}^2)c_W^4} \left\{ (m_{\tilde{\chi}_i^0}^2 - \hat{t})(m_{\tilde{\chi}_j^0}^2 - \hat{t}) \times [C_{\tilde{\chi}_i^0 \tilde{q}_k q}^L C_{\tilde{\chi}_i^0 \tilde{q}_l q}^{L*} + C_{\tilde{\chi}_i^0 \tilde{q}_k q}^R C_{\tilde{\chi}_i^0 \tilde{q}_l q}^{R*}] \times [C_{\tilde{\chi}_j^0 \tilde{q}_k q}^L C_{\tilde{\chi}_j^0 \tilde{q}_l q}^{L*} + C_{\tilde{\chi}_j^0 \tilde{q}_k q}^R C_{\tilde{\chi}_j^0 \tilde{q}_l q}^{R*}] \right\}, \quad (2.15)$$

$$M_{\hat{u}\hat{u}} = \sum_{k,l} \frac{4g^4}{(\hat{u} - m_{\tilde{q}_k}^2)(\hat{u} - m_{\tilde{q}_l}^2)c_W^4} \left\{ (m_{\tilde{\chi}_i^0}^2 - \hat{u})(m_{\tilde{\chi}_j^0}^2 - \hat{u}) \times [C_{\tilde{\chi}_i^0 \tilde{q}_k q}^{L*} C_{\tilde{\chi}_i^0 \tilde{q}_l q}^L + C_{\tilde{\chi}_i^0 \tilde{q}_k q}^{R*} C_{\tilde{\chi}_i^0 \tilde{q}_l q}^R] \times [C_{\tilde{\chi}_j^0 \tilde{q}_k q}^{L*} C_{\tilde{\chi}_j^0 \tilde{q}_l q}^L + C_{\tilde{\chi}_j^0 \tilde{q}_k q}^{R*} C_{\tilde{\chi}_j^0 \tilde{q}_l q}^R] \right\}, \quad (2.16)$$

$$M_{\hat{t}\hat{u}} = \sum_{k,l} \frac{4g^4}{(\hat{t} - m_{\tilde{q}_k}^2)(\hat{u} - m_{\tilde{q}_l}^2)c_W^4} \left\{ \frac{1}{2} [C_{\tilde{\chi}_i^0 \tilde{q}_k q}^{L*} C_{\tilde{\chi}_j^0 \tilde{q}_l q}^L C_{\tilde{\chi}_i^0 \tilde{q}_l q}^{R*} C_{\tilde{\chi}_j^0 \tilde{q}_k q}^R + C_{\tilde{\chi}_i^0 \tilde{q}_k q}^{L*} C_{\tilde{\chi}_j^0 \tilde{q}_k q}^L C_{\tilde{\chi}_i^0 \tilde{q}_l q}^{R*} C_{\tilde{\chi}_j^0 \tilde{q}_l q}^R] [(m_{\tilde{\chi}_i^0}^2 - \hat{u})(m_{\tilde{\chi}_j^0}^2 - \hat{u}) + (m_{\tilde{\chi}_i^0}^2 - \hat{t})(m_{\tilde{\chi}_j^0}^2 - \hat{t}) - \hat{s}(\hat{s} - m_{\tilde{\chi}_i^0}^2 - m_{\tilde{\chi}_j^0}^2)] + m_{\tilde{\chi}_i^0} m_{\tilde{\chi}_j^0} \hat{s} [C_{\tilde{\chi}_j^0 \tilde{q}_l q}^{L*} C_{\tilde{\chi}_i^0 \tilde{q}_k q}^L C_{\tilde{\chi}_j^0 \tilde{q}_k q}^{L*} C_{\tilde{\chi}_i^0 \tilde{q}_l q}^L + C_{\tilde{\chi}_j^0 \tilde{q}_l q}^{R*} C_{\tilde{\chi}_i^0 \tilde{q}_k q}^R C_{\tilde{\chi}_j^0 \tilde{q}_k q}^{R*} C_{\tilde{\chi}_i^0 \tilde{q}_l q}^R] \right\}, \quad (2.17)$$

$$M_{\hat{s}\hat{u}} = \sum_k \frac{2g^4 (Re[D_Z(\hat{s})])}{(\hat{u} - m_{\tilde{q}_k}^2)c_W^4} \left\{ [C_{Zqq}^L O_{ij}^{\prime\prime L*} C_{\tilde{\chi}_i^0 \tilde{q}_k q}^{L*} C_{\tilde{\chi}_j^0 \tilde{q}_k q}^L - C_{Zqq}^R O_{ij}^{\prime\prime L} C_{\tilde{\chi}_i^0 \tilde{q}_k q}^R C_{\tilde{\chi}_j^0 \tilde{q}_k q}^L] (m_{\tilde{\chi}_i^0}^2 - \hat{u})(m_{\tilde{\chi}_j^0}^2 - \hat{u}) + m_{\tilde{\chi}_i^0} m_{\tilde{\chi}_j^0} \hat{s} [C_{Zqq}^L O_{ij}^{\prime\prime L*} C_{\tilde{\chi}_i^0 \tilde{q}_k q}^{L*} C_{\tilde{\chi}_j^0 \tilde{q}_k q}^L - C_{Zqq}^R O_{ij}^{\prime\prime L} C_{\tilde{\chi}_i^0 \tilde{q}_k q}^R C_{\tilde{\chi}_j^0 \tilde{q}_k q}^L] \right\}, \quad (2.18)$$

$$M_{\hat{s}\hat{t}} = \sum_k \frac{2g^4 (Re[D_Z(\hat{s})])}{(\hat{t} - m_{\tilde{q}_k}^2)c_W^4} \left\{ [C_{Zqq}^R O_{ij}^{\prime\prime L*} C_{\tilde{\chi}_i^0 \tilde{q}_k q}^{R*} C_{\tilde{\chi}_j^0 \tilde{q}_k q}^R - C_{Zqq}^L O_{ij}^{\prime\prime L} C_{\tilde{\chi}_i^0 \tilde{q}_k q}^L C_{\tilde{\chi}_j^0 \tilde{q}_k q}^R] (m_{\tilde{\chi}_i^0}^2 - \hat{t})(m_{\tilde{\chi}_j^0}^2 - \hat{t}) + m_{\tilde{\chi}_i^0} m_{\tilde{\chi}_j^0} \hat{s} [C_{Zqq}^L O_{ij}^{\prime\prime L*} C_{\tilde{\chi}_i^0 \tilde{q}_k q}^{L*} C_{\tilde{\chi}_j^0 \tilde{q}_k q}^L - C_{Zqq}^R O_{ij}^{\prime\prime L} C_{\tilde{\chi}_i^0 \tilde{q}_k q}^R C_{\tilde{\chi}_j^0 \tilde{q}_k q}^R] \right\}, \quad (2.19)$$

where $D_Z(\hat{s})$ is propagator of the Z^0 boson.

For obtaining the total cross section of the subprocess we use the following formula:

$$\hat{\sigma}(\hat{s}) = \int_{\hat{t}^-}^{\hat{t}^+} d\hat{t} \frac{d\hat{\sigma}}{d\hat{t}}, \quad (2.20)$$

where the upper and lower bounds of integral are defined as $\hat{t}^\pm = 1/2[(m_i^2 + m_j^2 - \hat{s}) \pm \sqrt{(\hat{s} - m_i^2 - m_j^2)^2 - 4m_i^2 m_j^2}]$. Once the cross section for the partonic process has been computed, the total hadronic cross sections in proton-proton collisions in terms of the center-of-mass energy could be readily obtained using

$$\sigma(s) = \int_{(m_{\tilde{\chi}_i^0} + m_{\tilde{\chi}_j^0})^2/s}^1 d\tau \frac{d\mathcal{L}_{ab}^{AB}}{d\tau} \hat{\sigma}(\text{subprocess, at } \hat{s} = \tau s), \quad (2.21)$$

with the parton luminosity

$$\frac{d\mathcal{L}_{ab}^{AB}}{d\tau} = \int_{\tau}^1 \frac{dx_1}{x_1} \frac{1}{1 + \delta_{ab}} \left[G_{a/A}(x_1, \mu_F) G_{b/B}\left(\frac{\tau}{x_1}, \mu_F\right) + G_{b/A}(x_1, \mu_F) G_{a/B}\left(\frac{\tau}{x_1}, \mu_F\right) \right], \quad (2.22)$$

where the universal parton distribution functions (PDFs) for the partons a, b , constituents of hadrons A, B are denoted by $G_{a/A}$ and $G_{b/B}$, depending on the longitudinal momentum fractions of the two partons x_1, x_2 ($\tau = x_1 x_2$) at a factorization scale μ_F . During our calculations, the factorization scale is chosen as the average mass of the produced particles, namely, $\mu_F = (m_{\tilde{\chi}_i^0} + m_{\tilde{\chi}_j^0})/2$.

III. ONE-LOOP CONTRIBUTIONS TO THE NEUTRALINO PAIR PRODUCTION

At the one-loop level production of neutralino pair is proceeded via quark-antiquark annihilation and gluon-gluon fusion in the hadron colliders. Feynman diagrams for the one-loop contributions to the process $pp \rightarrow \tilde{\chi}_i^0 \tilde{\chi}_j^0$ can be divided into three kind diagrams as follows: The box diagrams, the self energy corrections diagrams, and triangle diagrams. Any one-loop amplitude could be given as a linear sum of triangle, box, bubble, and tadpole one-loop integrals.

In the numerical calculations of high-energy processes observed at the current and future accelerators such as LHC and ILC, for precise theoretical predictions of cross sections one needs to include higher-order corrections. In the common case it is explained in the following: First of all, the lowest-order approximation in perturbative calculations of high energy physics is not sufficiently accurate to be compared to the experimental data. Thus, it is important to consider the contributions from higher-order terms as well. For including these corrections in the Standard model or beyond, it is indispensable to handle the evaluation of loop integrals.

We briefly describe the general properties of the box, triangle and self energy corrections diagrams in the following part. The general form the triangle diagram in four dimensions is proportional to the antisymmetric tensor $\varepsilon_{\mu\nu\rho\sigma}$. Such tensor could not be continued to general

dimensions, because it has exactly four indices. Therefore, such diagram is excluded from the general proof and has to be treated separately via a different regularization scheme, e.g. the Pauli-Villars method. It must be verified that all higher-order diagrams including the $\varepsilon_{\mu\nu\rho\sigma}$ tensor may be renormalized without demolishing gauge invariance. One of the main conditions for the proof of renormalizability, in general, is that this scheme should be gauge invariant and the Slavnov-Taylor identities can be established.

In our case self-energy diagrams consist of the quark, squark, and boson self-energy corrections. These contributions have different properties. It should be noted that the self-energy of the fermions is not physically observable, and therefore it does not make sense even if it has the logarithmic divergence. The basic problem should appear when there is a logarithmic divergence in the evaluation of the physical observable. The most important example is the vertex correction due to the photon or gluon propagation. If it has a logarithmic divergence, then it should be renormalized into the wave function.

We have performed numerical calculations in the 't Hooft-Feynman gauge where the gluon polarization sum is given by $\sum_{\lambda} \epsilon_{\mu}^*(k, \lambda) \epsilon_{\nu}(k, \lambda) = -g_{\mu\nu}$. We have considered the constrained differential renormalization (CDR) [25] with a view to regularize the ultraviolet (UV) divergences. At the one-loop level, the CDR has been presented to be equivalent to the regularization by dimensional reduction [26, 27], which is a modified version of dimensional regularization. Hence, a supersymmetry-preserving regularization scheme is supplied by the implementation given in Ref. [28]. For a treatment of the appearing infrared (IR) and collinear singularities we use mass regularization, such as IR singularities are treated by a small gluon mass, and the masses of the light quarks are kept in collinearly singular integrals.

We do not give the analytical results for the one-loop level since these are too long to be included here. Now we give kinematic expressions and the Feynman diagrams for the neutralino pair production in the next subsections, considering each partonic process separately.

A. The partonic process $q\bar{q} \rightarrow \tilde{\chi}_i^0 \tilde{\chi}_j^0$ in the one-loop level

The Feynman diagrams contributing to the subprocess $q\bar{q} \rightarrow \tilde{\chi}_i^0 \tilde{\chi}_j^0$ in the one-loop level are depicted from Fig. 2 to 4. The virtual corrections to this process include the following generic structure of one-loop Feynman diagrams: Self-energy, three-point vertex and box corrections as shown in Figs. 2, 3 and 4, respectively. In these figures the label S^0 represents all neutral Higgs bosons h^0, H^0, A^0, G^0 , and the label \tilde{f}_m^w (f_m) refers to scalar fermions (fermions) $\tilde{e}_m^w, \tilde{u}_m^w, \tilde{d}_m^w$ (e_m, ν_m, u_m, d_m). The subscript m and superscripts w, x, y refer to the generation of (s)quark and the squark mass eigenstates, respectively.

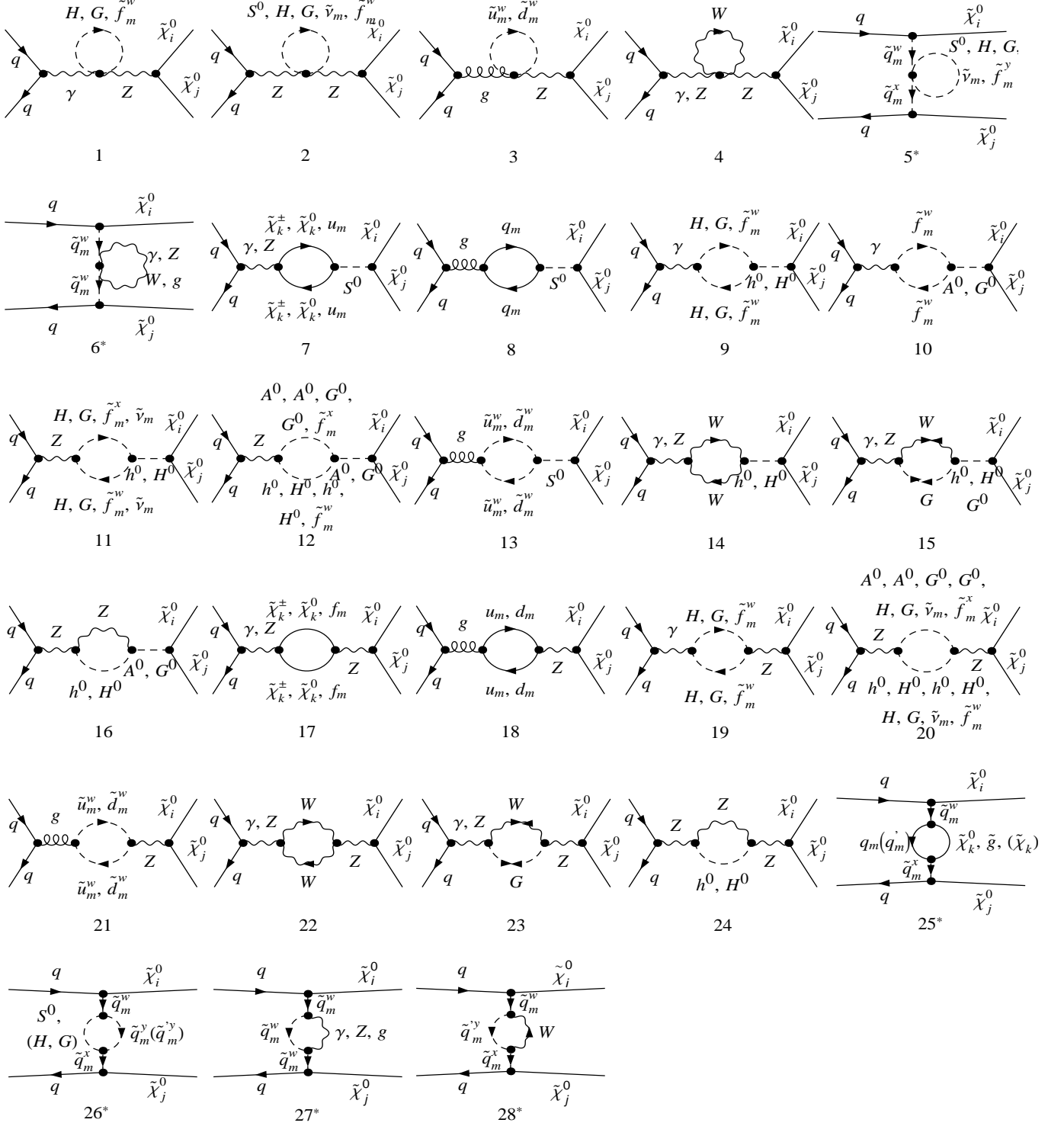


FIG. 2. Feynman diagrams for self-energy corrections to neutralino pair production via $q\bar{q} \rightarrow \tilde{\chi}_i^0 \tilde{\chi}_j^0$ to one-loop level. Here, the diagrams with exchanging the final state neutralinos in the t -channel diagrams are not explicitly shown. The star on the numbers under some diagrams refers to the t -channel diagrams.

We denote the process of neutralino pair production via quark-antiquark annihilation as

$$q(p_1)\bar{q}(p_2) \rightarrow \tilde{\chi}_i^0(k_1)\tilde{\chi}_j^0(k_2), \quad (3.1)$$

where the labels in parentheses represent the four momenta of the corresponding particles.

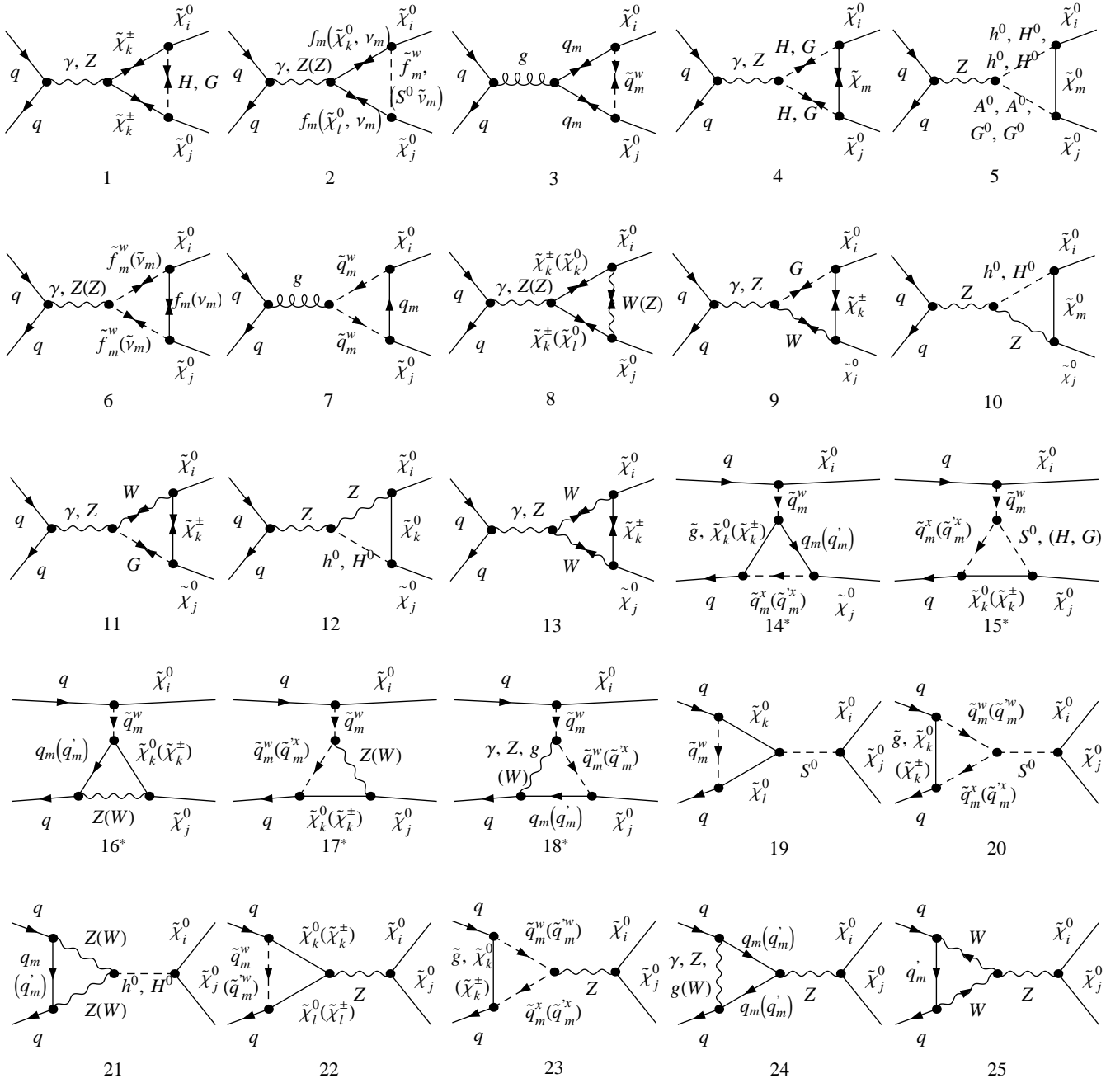


FIG. 3. Feynman diagrams for vertex corrections to neutralino pair production via $q\bar{q} \rightarrow \tilde{\chi}_i^0 \tilde{\chi}_j^0$ to one-loop level. Also, this subprocess contains diagrams which have corrections in the neutral vertex including the same $\tilde{\chi}_i^0 \tilde{\chi}_j^0$ corrections in the diagrams from 14 to 18. Here, the diagrams with exchanging the final state neutralinos in the t -channel diagrams are not explicitly shown. The star on the numbers under some diagrams refers to the t -channel diagrams.

B. The partonic process $g\bar{g} \rightarrow \tilde{\chi}_i^0 \tilde{\chi}_j^0$ in the one-loop level

The subprocess $g\bar{g} \rightarrow \tilde{\chi}_i^0 \tilde{\chi}_j^0$ in the lowest order can only be produced by way of one-loop diagrams, namely it does not emerge at the tree level. We represent the process of

neutralino pair production via gluon-gluon fusion with

$$g(p_3)g(p_4) \rightarrow \tilde{\chi}_i^0(k_3)\tilde{\chi}_j^0(k_4), \quad (3.2)$$

where the labels in parentheses represent the four momenta of the relevant particles. The Mandelstam vari-

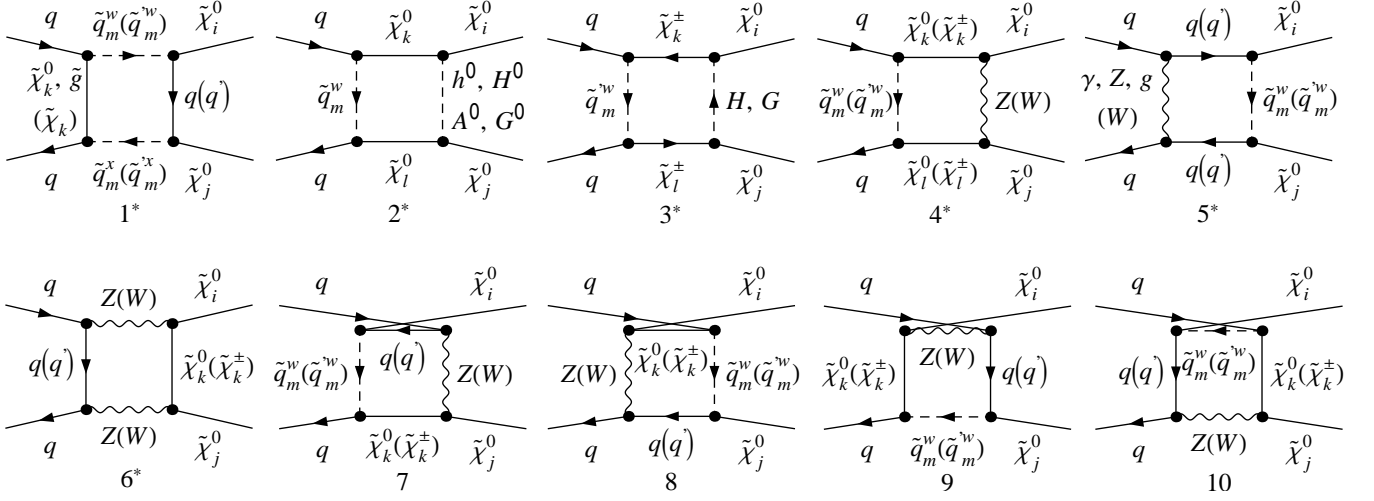


FIG. 4. Feynman diagrams for box corrections to neutralino pair production via $q\bar{q} \rightarrow \tilde{\chi}_i^0 \tilde{\chi}_j^0$ to one-loop level. Here, the diagrams with exchanging the final state neutralinos in the t -channel diagrams are not explicitly shown. The star on the numbers under some diagrams refers to the t -channel diagrams.

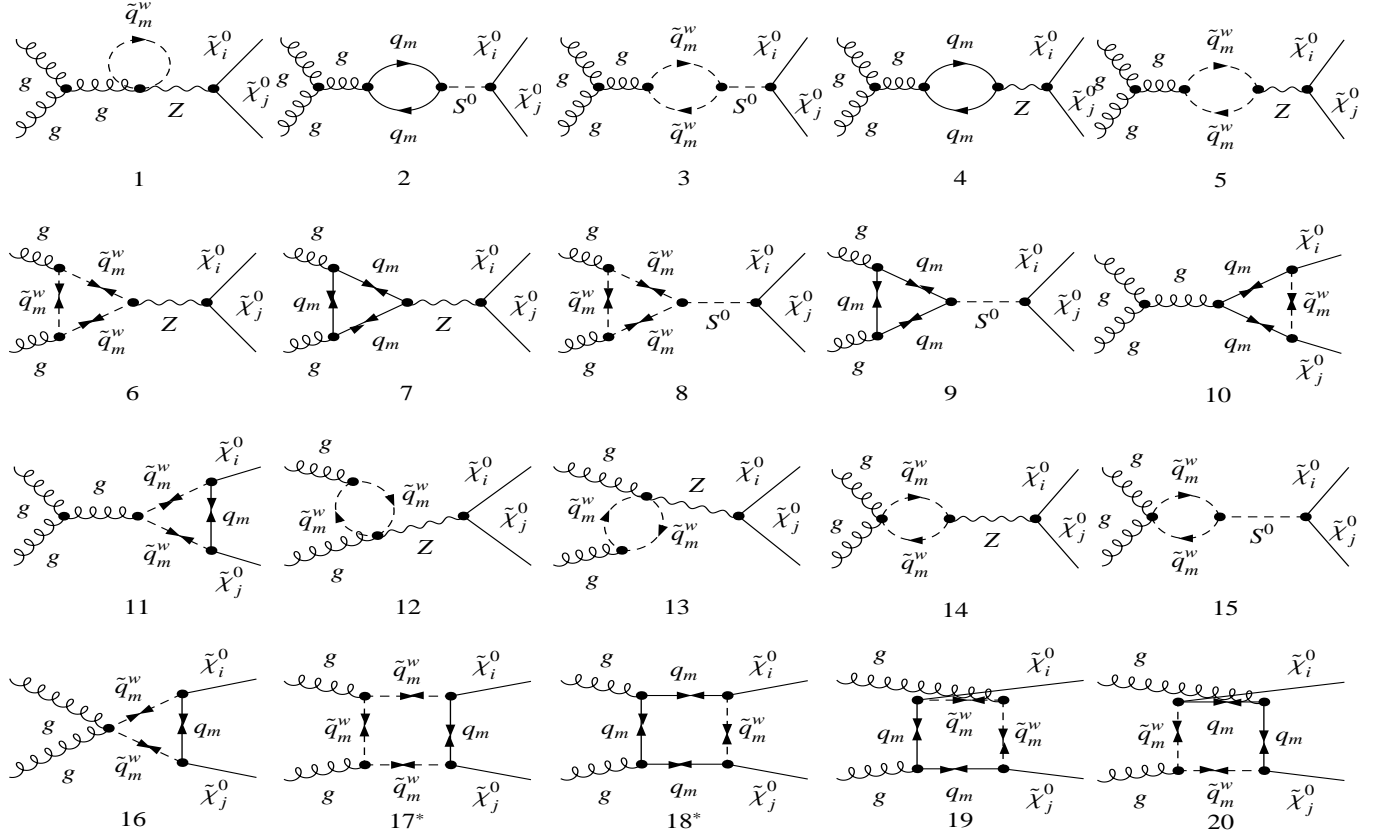


FIG. 5. Feynman diagrams for virtual corrections to neutralino pair production via $gg \rightarrow \tilde{\chi}_i^0 \tilde{\chi}_j^0$ to one-loop level. Here, the diagrams with crossed final states are not explicitly shown. The subscript m and superscripts w refer to the generation of (s)quark and the squark mass eigenstates, respectively.

ables for subprocess (3.2) are given by

$$\hat{s} = (p_3 + p_4)^2, \quad \hat{t} = (p_3 - k_3)^2, \quad \hat{u} = (p_3 - k_4)^2. \quad (3.3)$$

For this process, there is no need to take into account the renormalization at the one-loop level and provided

that all of the one-loop contributions are involved in the MSSM, the UV divergence will automatically be canceled. The Feynman diagrams contributing to the subprocess $gg \rightarrow \tilde{\chi}_i^0 \tilde{\chi}_j^0$ in the one-loop level are depicted in Fig. 5. The virtual corrections to this process include the following generic structure of one-loop Feynman diagrams: Self-energy, vertex and box corrections as shown in diagrams from 1 to 5, 6 to 15 and 16 to 20 in Fig. 5, respectively. As seen from these diagrams, this process involves virtual quark/squark corrections. In this figure all neutral Higgs bosons h^0, H^0, A^0, G^0 are denoted by the label S^0 and the star on the numbers under some diagrams represents that these are t-channel diagrams.

IV. PARAMETER SPACE

We now give the information about our method and input parameters used in the numerical analysis. During our numerical evaluations, we take into account the assumptions and approaches in our previous paper [29] for the gaugino/Higgsino sector. The soft SUSY-breaking gaugino mass parameters M_1, M_2 and the Higgsino mass parameter μ can be taken to be real and positive. These gaugino mass parameters are commonly supposed to be connected by way of the relation $M_1 = \frac{5}{3}M_2 \tan^2 \theta_W \simeq 0.5M_2$. The parameters M_2 and μ are obtained as shown in Eqs. (A13) and (A14) in Ref. [29] by taking the suitable differences and sums of the chargino masses. Consequently, there appear three different cases in the selection of the gaugino/Higgsino mass parameters M_2 and μ . These are the Higgsino-like, gauginolike, and mixture-case, separately. We can refer the reader to Ref. [29] for further details. We set the chargino masses as

$$m_{\tilde{\chi}_1^\pm} = 168.51 \text{ GeV}, m_{\tilde{\chi}_2^\pm} = 295.01 \text{ GeV} \quad (4.1)$$

for both Higgsino-like and gauginolike scenarios, and

$$m_{\tilde{\chi}_1^\pm} = 173.66 \text{ GeV}, m_{\tilde{\chi}_2^\pm} = 289.86 \text{ GeV} \quad (4.2)$$

for mixture-case scenario. Then, the parameters μ and M_2 related to the scenarios are calculated from these values in (4.1) and (4.2) for given $\tan \beta$. Furthermore, neutralino masses for each scenario are obtained by inserting the values of μ and M_2 into Eq. (A8) in Ref. [29]. Taking into account the constraint on SUSY parameters from recent experiments [11–13], we set the soft SUSY-breaking parameters for the entries of mass matrices in the sfermion sector to be equal as $M_{SUSY} = 1.5 \text{ TeV}$. We get the other SUSY parameters as follows:

$$\begin{aligned} \tan \beta &= 45, m_{A^0} = 2.5 \text{ TeV}, \\ A_t &= A_b = A_\tau = \mu / \tan \beta + 2M_{SUSY}, \\ m_{\tilde{u}_L} &= 1499.02 \text{ GeV}, m_{\tilde{u}_R} = 1499.59 \text{ GeV}, \\ m_{\tilde{d}_L} &= 1500.18 \text{ GeV}, m_{\tilde{d}_R} = 1501.20 \text{ GeV}, \\ m_{\tilde{g}} &= 1500 \text{ GeV}, \end{aligned} \quad (4.3)$$

where $A_{t,b,\tau}$ are the trilinear couplings and m_{A^0} is the mass of the neutral CP-odd Higgs boson. Furthermore, we take the following input parameters for the SM, $m_Z = 91.1876 \text{ GeV}$, $m_W = 80.399 \text{ GeV}$, $\alpha^{-1} = 137.036$, $\alpha(m_Z^2)^{-1} = 127.934$ and $\alpha_s(m_Z^2) = 0.1184$ [17], and we ignore the masses of the light quarks. The running strong coupling $\alpha_s(\mu_0^2)$ at energy scale $\mu_0 = (m_{\tilde{\chi}_1^0} + m_{\tilde{\chi}_1^0})/2$ yields 0.1152, 0.1183, and 0.1165 in the Higgsino-like scenario, gauginolike scenario, and mixture-case scenario, respectively.

Additionally, we have considered the CMSSM 40.2.4 benchmark point [30] in order to make the comparison with our scenarios. The CMSSM [31–33] contains five input parameters, namely, the universal trilinear soft SUSY breaking parameter A_0 , the universal scalar mass parameter m_0 , gaugino mass parameter $m_{1/2}$, the ratio of the expectation values of the two Higgs doublets $\tan \beta$ and the sign of the Higgs mixing parameter $\text{sign}(\mu)$. It is believed that the universal parameters A_0, m_0 , and $m_{1/2}$ arise via some gravity-mediated mechanism, and these are defined at the grand unified theories scale while $\text{sign}(\mu)$ and $\tan \beta$ are described at the electroweak scale. In the CMSSM 40.2.4 benchmark point, the input parameters are given as follows: $m_0 = 700 \text{ GeV}$, $m_{1/2} = 600 \text{ GeV}$, $A_0 = -500 \text{ GeV}$, $\tan \beta = 40$, and $\mu > 0$. In this case, we obtain the corresponding SUSY particle spectrum with the help of `SoftSusy-3.3.9` package [34] as follows:

$$\begin{aligned} m_{\tilde{\chi}_1^\pm} &= 480.02 \text{ GeV}, m_{\tilde{\chi}_2^\pm} = 809.62 \text{ GeV}, \\ m_{\tilde{u}_L} &= 1413.98 \text{ GeV}, m_{\tilde{u}_R} = 1374.64 \text{ GeV}, \\ m_{\tilde{d}_L} &= 1416.06 \text{ GeV}, m_{\tilde{d}_R} = 1370.96 \text{ GeV}, \\ m_{\tilde{g}} &= 1384.44 \text{ GeV}, m_{h^0} = 118.04 \text{ GeV}, \\ m_{A^0} &= m_{H^0} = 807.41 \text{ GeV}. \end{aligned} \quad (4.4)$$

Furthermore, Table I shows a list of the Higgsino/gaugino mass parameters, neutralino masses, and $\tan \beta$ for our scenarios and the CMSSM 40.2.4 benchmark point.

V. NUMERICAL RESULTS AND DISCUSSION

Let us now discuss in detail the numerical predictions of the process $pp \rightarrow \tilde{\chi}_i^0 \tilde{\chi}_j^0$ at the LHC energies, taking into account the full one-loop contributions from quark-antiquark annihilation and gluon-gluon fusion. We carry out the numerical evaluation using the Mathematica packages `FEYNARTS` [35] to obtain the relevant amplitudes, `FORMCALC` [36] to supply both the analytical results and a complete Fortran code for numerical evaluation of the squared matrix elements, and `LOOPTOOLS` [37] to make the evaluation of the necessary loop integrals as based on Passarino-Veltman reduction techniques [38]. In addition, with the help of `FEYNARTS` we generate all relevant Feynman diagrams, which are shown in Figs. 1 through 5. Higgs properties are computed by using `FEYNHIGGS` [39].

TABLE I. The Higgsino/gaugino mass parameters, neutralino masses, and $\tan\beta$ for each scenario, where all mass parameters are in GeV.

	M_2	μ	M_1	$\tan\beta$	$m_{\tilde{\chi}_1^0}$	$m_{\tilde{\chi}_2^0}$	$m_{\tilde{\chi}_3^0}$	$m_{\tilde{\chi}_4^0}$
Higgsino-like	250.00	200.00	119.33	45.00	109.59	174.50	209.65	294.88
Gauginolike	200.00	250.00	95.46	45.00	91.50	169.50	259.40	293.85
Mixture case	225.00	225.00	107.39	45.00	101.42	176.13	234.52	289.37
CMSSM 40.2.4	470.87	795.94	254.88	40.00	251.96	479.89	800.38	808.69

In the numerical treatment, we use the MSTW2008 PDFs [40] interfaced via the LHAPDF package [41] for the distribution of the gluon/quark in the proton. Moreover, we set the central renormalization and factorization scales to be equal ($\mu_0 = \mu_F = \mu_R$) and fix μ_0 as the average mass of the produced particles $\mu_0 = (m_{\tilde{\chi}_i^0} + m_{\tilde{\chi}_j^0})/2$ in default. To have a quantitative understanding of the effects of one-loop contributions on the neutralino pair production, it is convenient to compute the K factor, which is defined as the ratio between the total NLO and LO cross sections, namely, $K = (\sigma_{NLO}^{q\bar{q}} + \sigma_{NLO}^{gg})/\sigma_{LO}$.

For representative parameter points of each of the scenarios defined in Table I, we have performed numerical evaluation of the total Born cross sections σ_{LO} , the one-loop cross sections for quark-antiquark annihilation and gluon-gluon fusion $\sigma_{NLO}^{q\bar{q}/gg}$, and the K factor, as a function of the center-of-mass energy from Figs. 6 through 8, the M_2 - μ mass plane from Figs. 9 through 11, the squark mass from Figs. 12 through 14, and the factorization scale from Figs. 15 through 17. However, the neutralino masses and mixing matrix are not very sensitive with respect to variation of the $\tan\beta$, so we do not illustrate any plots against it. In order to display the numerical effect of the NLO contributions on the LO cross section, we show the associated K factor in the lower part of some plots. In these figures, the solid curves denote the Born cross sections, and the dashed and dash-dotted curves represent the one-loop cross sections for quark-antiquark annihilation and gluon-gluon fusion, respectively. We use the following abbreviations: GL, gauginolike; HL, Higgsino-like; MC, mixture case, and 40.2.4, CMSSM 40.2.4 benchmark point. Now we present separately the following detailed analysis of these figures.

In Figs. 6 to 8, the dependence of the total LO cross sections, the NLO cross sections and the K factors on the center-of-mass energy are plotted. These plots indicate that both LO and NLO cross sections increase smoothly and slowly with increasing the center-of-mass energy for each scenario. Moreover, the corresponding K factors grow by about 1 percent when the center-of-mass energy increase from 7 to 14 TeV. It implies that the K factor is less sensitive according to varying the center-of-mass energy. As shown in Fig. 6, the LO cross section of the process $pp \rightarrow \tilde{\chi}_1^0 \tilde{\chi}_1^0$ in the Higgsino-like scenario is roughly 41%, 64%, and one order of magnitude larger than in the mixture-case scenario, gauginolike scenario, and CMSSM 40.2.4 benchmark point, respectively. The

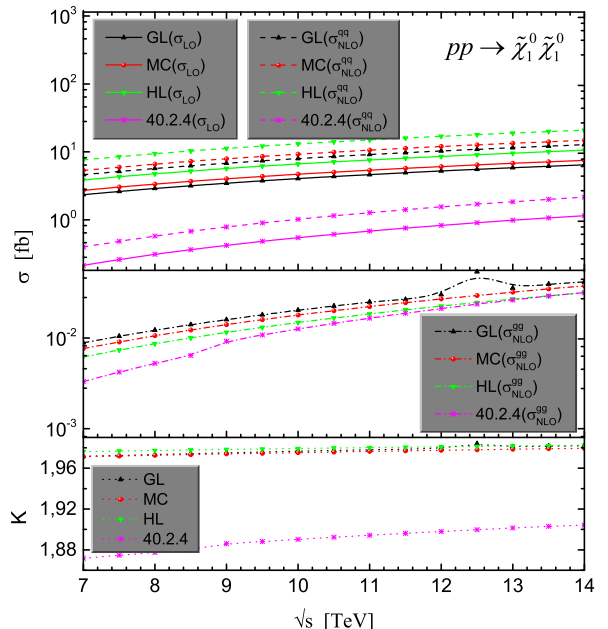


FIG. 6. (color online). Total LO and NLO cross sections of the process $pp \rightarrow \tilde{\chi}_1^0 \tilde{\chi}_1^0$ versus the center-of-mass energy of pp collider. The lower panel shows the K factor, $K = (\sigma_{NLO}^{q\bar{q}} + \sigma_{NLO}^{gg})/\sigma_{LO}$.

K factors of the process $pp \rightarrow \tilde{\chi}_1^0 \tilde{\chi}_1^0$ in our scenarios are nearly equal to each other, while they are 5% larger than in the CMSSM 40.2.4 benchmark point. Furthermore, one can see from Fig. 7 that the LO cross section of the process $pp \rightarrow \tilde{\chi}_1^0 \tilde{\chi}_2^0$ in the Higgsino-like scenario is enhanced by about 26%, 70%, and two orders of magnitude relative to the mixture-case scenario, the gauginolike scenario, and CMSSM 40.2.4 benchmark point, respectively. The K factors for this process in our scenarios are approximately equal to each other, while they are 7% larger than in the CMSSM 40.2.4 benchmark point. Finally, in Fig. 8, the LO cross section of the process $pp \rightarrow \tilde{\chi}_2^0 \tilde{\chi}_2^0$ in the gauginolike scenario is enhanced by around 65%, 3 times of magnitude, and 7 times of magnitude relative to the mixture-case scenario, Higgsino-like scenario, and CMSSM 40.2.4 benchmark point, respectively. The K factor for this process in the Higgsino-like scenario is roughly 1%, 1%, and 5% larger than in the mixture-case scenario, gauginolike scenario, and CMSSM 40.2.4 benchmark point, respectively.

TABLE II. Total LO, NLO cross sections (in fb) and corresponding K factors at center-of-mass energy $\sqrt{s} = 8$ and 14 TeV for each scenario. Here the K factor is $K = (\sigma_{NLO}^{qq} + \sigma_{NLO}^{gg})/\sigma_{LO}$.

scenario	\sqrt{s} [TeV]	$pp \rightarrow \tilde{\chi}_1^0 \tilde{\chi}_1^0$				$pp \rightarrow \tilde{\chi}_1^0 \tilde{\chi}_2^0$				$pp \rightarrow \tilde{\chi}_2^0 \tilde{\chi}_2^0$			
		σ_{LO}	σ_{NLO}^{qq}	σ_{NLO}^{gg}	K	σ_{LO}	σ_{NLO}^{qq}	σ_{NLO}^{gg}	K	σ_{LO}	σ_{NLO}^{qq}	σ_{NLO}^{gg}	K
Higgsino-like	8	4.76	9.40	0.009	1.98	0.85	1.70	$1.3 \cdot 10^{-4}$	2.00	0.99	1.96	0.007	1.99
	14	10.54	20.87	0.032	1.98	1.95	3.90	$5.4 \cdot 10^{-4}$	2.00	2.71	5.38	0.029	2.00
Gauginolike	8	2.89	5.70	0.012	1.97	0.51	1.01	$1.8 \cdot 10^{-6}$	1.99	2.75	5.36	0.028	1.96
	14	6.45	12.74	0.042	1.98	1.11	2.22	$7.2 \cdot 10^{-6}$	2.00	7.78	15.25	0.124	1.98
Mixture case	8	3.35	6.60	0.011	1.97	0.68	1.36	$2.7 \cdot 10^{-5}$	1.99	1.93	3.77	0.014	1.97
	14	7.49	14.79	0.038	1.98	1.53	3.05	$1.2 \cdot 10^{-4}$	1.99	5.35	10.53	0.065	1.98
CMSSM 40.2.4	8	0.31	0.58	0.005	1.88	0.01	0.02	$1.2 \cdot 10^{-9}$	1.87	0.27	0.51	0.007	1.92
	14	1.15	2.15	0.032	1.90	0.04	0.08	$1.5 \cdot 10^{-7}$	1.88	1.63	3.11	0.071	1.95

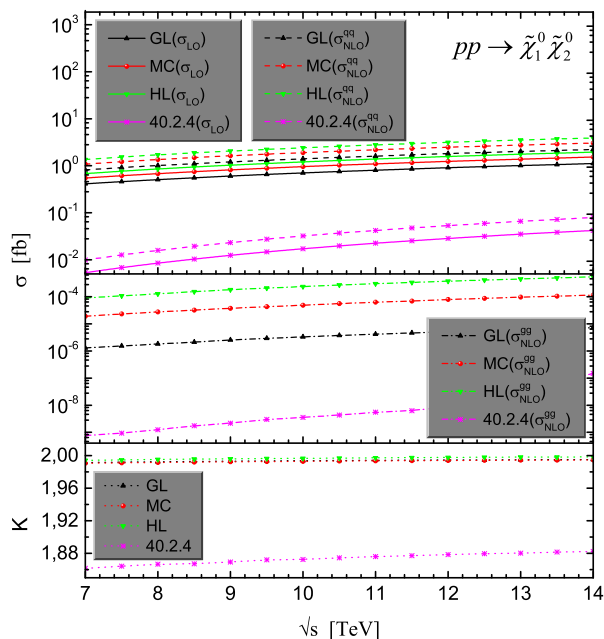


FIG. 7. (color online). Total LO and NLO cross sections of the process $pp \rightarrow \tilde{\chi}_1^0 \tilde{\chi}_1^0$ versus the center-of-mass energy of pp collider. The lower panel shows the K factor, $K = (\sigma_{NLO}^{qq} + \sigma_{NLO}^{gg})/\sigma_{LO}$.

We document a numerical survey over our scenarios and the CMSSM 40.2.4 benchmark point for LHC center-of-mass energies of 8 and 14 TeV in Table II. One can deduce from above analysis and this table that the total LO and NLO cross section of the process $pp \rightarrow \tilde{\chi}_1^0 \tilde{\chi}_1^0$ in the Higgsino-like scenario is usually larger than others. The LO (NLO) cross section of the process $pp \rightarrow \tilde{\chi}_1^0 \tilde{\chi}_1^0$ in the Higgsino-like scenario appears in the range of 3.9 to 10.5 ($\sigma_{NLO} = 7.6$ to 20.9) fb, resulting in K factor of about $K = 1.98$. Furthermore, for process $pp \rightarrow \tilde{\chi}_2^0 \tilde{\chi}_2^0$ in the gauginolike scenario, the cross section appears in the range of 2.07 to 7.8 ($\sigma_{NLO} = 4.05$ to 15.4) fb, resulting in K factor of $K = 1.96$ to 1.98 and should be observable at LHC. The quark-antiquark annihila-

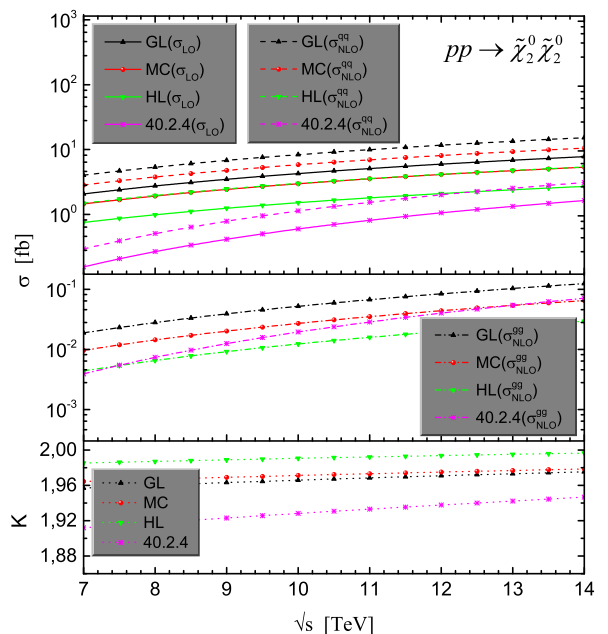


FIG. 8. (color online). Total LO and NLO cross sections of the process $pp \rightarrow \tilde{\chi}_2^0 \tilde{\chi}_2^0$ versus the center-of-mass energy of pp collider. The lower panel shows the K factor, $K = (\sigma_{NLO}^{qq} + \sigma_{NLO}^{gg})/\sigma_{LO}$.

tion yields larger NLO cross section than gluon-gluon fusion for each scenario. The sizes of the NLO cross sections are at a visible level of 10^{-1} fb for gg fusion while 10^1 fb for $q\bar{q}$ annihilation. Particularly, for process $gg \rightarrow \tilde{\chi}_2^0 \tilde{\chi}_2^0$ in the gauginolike scenario, the cross section reaches a value of 0.124 fb at $\sqrt{s} = 14$ TeV. Moreover, as one sees from Table II, the NLO contributions for neutralino pair production are so significant that the K factor yields around $K \sim 2$. One notes that the associated K factors barely change between our scenarios according to the dependence on the center-of-mass energy. This behavior between K factors is shown to be ordered as $HL(K) \sim GL(K) \sim MC(K) > CMSSM(K)$.

The neutralino/chargino masses and mixing matrices

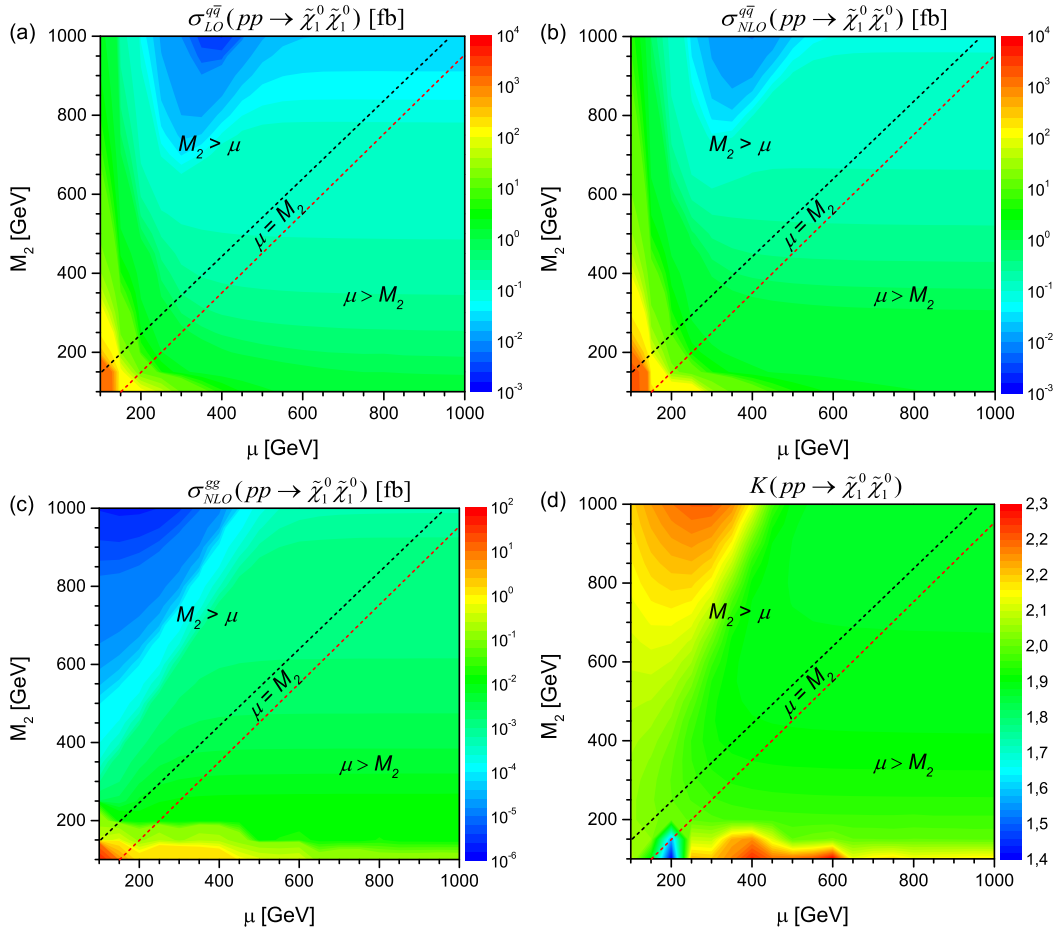


FIG. 9. (color online). Contour plots of the total (a) LO, (b)-(c) NLO cross sections and (d) K factor of the process $pp \rightarrow \tilde{\chi}_1^0 \tilde{\chi}_1^0$ in the $M_2 - \mu$ plane for $\sqrt{s} = 8$ TeV, where we take $\tan \beta = 45$ and fix $M_1 = \frac{5}{3} M_2 \tan^2 \theta_W$.

depend on the M_2 and μ mass parameters so significantly that the interesting information can be obtained from the dependence of the cross section on these parameters. Correspondingly, we investigate the effect of these parameters on the LO, NLO cross sections and the K factors of the relevant process in $M_2 - \mu$ mass plane with varying these parameters in the range from 100 to 1000 GeV in steps of 50 GeV at $\sqrt{s} = 8$ TeV for $\tan \beta = 45$, as illustrated in Figs. 9 through 11. In these plots, the region below the red dashed line corresponds to gauginolike ($\mu > M_2$), the region above the black dashed line corresponds to Higgsino-like ($M_2 > \mu$), and the region between the two dashed lines corresponds to mixture case ($\mu = M_2$). One sees that the LO and NLO cross sections increase with decreasing M_2 and any value of μ for $pp \rightarrow \tilde{\chi}_1^0 \tilde{\chi}_1^0$ and $pp \rightarrow \tilde{\chi}_2^0 \tilde{\chi}_2^0$, whereas decreasing μ and any value of M_2 for $pp \rightarrow \tilde{\chi}_1^0 \tilde{\chi}_2^0$. In particular, cross section reaches maximal values in the region $M_2 \lesssim 400$ GeV for $pp \rightarrow \tilde{\chi}_1^0 \tilde{\chi}_1^0$ and $\tilde{\chi}_2^0 \tilde{\chi}_2^0$, and $\mu \lesssim 500$ GeV for $pp \rightarrow \tilde{\chi}_1^0 \tilde{\chi}_2^0$ into the scan region. From these results one can conclude that pure gaugino couplings dominate in the case of same type of neutralinos $i = j$, whereas pure

Higgsino couplings enhance in the case of different type of neutralinos $i \neq j$ for $pp \rightarrow \tilde{\chi}_i^0 \tilde{\chi}_j^0$. The K factors have mostly the values in the range between 2.3 to 1.8 for $pp \rightarrow \tilde{\chi}_1^0 \tilde{\chi}_1^0$ [shown in Fig. 9(d)], 2.0 to 1.8 for $pp \rightarrow \tilde{\chi}_1^0 \tilde{\chi}_2^0$ [shown in Fig. 10(d)] and 2.2 to 1.9 for $pp \rightarrow \tilde{\chi}_2^0 \tilde{\chi}_2^0$ [shown in Fig. 11(d)] in the scan region. The maximum values of the K factor are obtained in the region $\mu \lesssim 500$ GeV and $400 \lesssim M_2 \lesssim 1000$ GeV for processes $pp \rightarrow \tilde{\chi}_1^0 \tilde{\chi}_1^0$, $\mu \lesssim 500$ GeV and $M_2 \lesssim 500$ GeV for processes $pp \rightarrow \tilde{\chi}_1^0 \tilde{\chi}_2^0$ and $\mu > M_2$ for process $pp \rightarrow \tilde{\chi}_2^0 \tilde{\chi}_2^0$. For example the K factor increases from 1.45 to 2.22 for $pp \rightarrow \tilde{\chi}_1^0 \tilde{\chi}_1^0$, whereas decreases from 2.01 to 1.93 for $pp \rightarrow \tilde{\chi}_1^0 \tilde{\chi}_2^0$ and 1.99 to 1.44 for $pp \rightarrow \tilde{\chi}_2^0 \tilde{\chi}_2^0$ with the increment of M_2 from 100 to 1000 GeV at $\mu = 200$ GeV. What's more, when the parameter μ varies from 100 to 1000 GeV for $M_2 = 200$ GeV, the K factor decreases from 2.02 to 1.94 for $pp \rightarrow \tilde{\chi}_1^0 \tilde{\chi}_1^0$, from 2.03 to 1.90 for $pp \rightarrow \tilde{\chi}_1^0 \tilde{\chi}_2^0$ and from 1.94 to 1.93 for $pp \rightarrow \tilde{\chi}_2^0 \tilde{\chi}_2^0$. As a consequence, it is clearly visible that the K factor strongly depends on the parameters M_2 and μ .

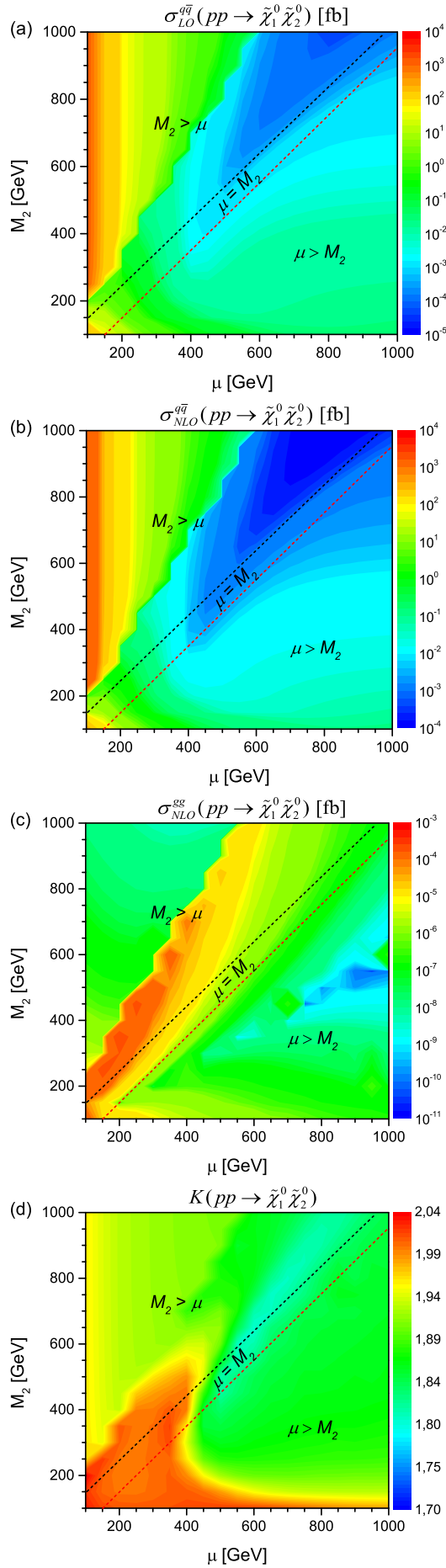


FIG. 10. (color online). Contour plots of the total (a) LO, (b)-(c) NLO cross sections and (d) K factor of the process $pp \rightarrow \tilde{\chi}_1^0 \tilde{\chi}_2^0$ in the $M_2 - \mu$ plane for $\sqrt{s} = 8$ TeV, where we take $\tan \beta = 45$ and fix $M_1 = \frac{5}{3} M_2 \tan^2 \theta_W$.

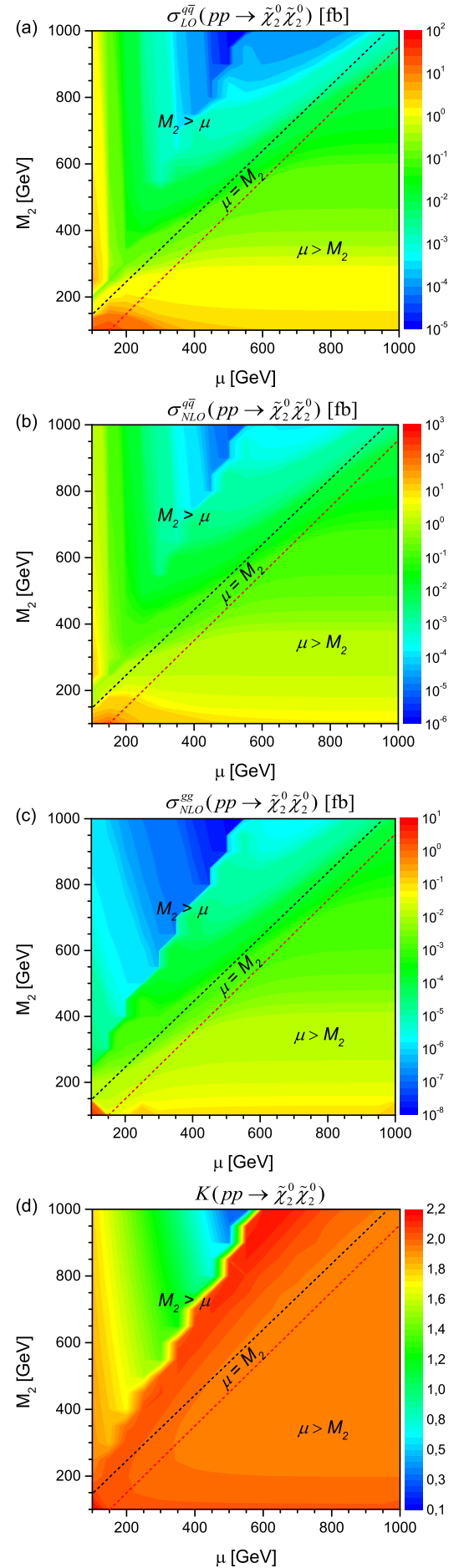


FIG. 11. (color online). Contour plots of the total (a) LO, (b)-(c) NLO cross sections and (d) K factor of the process $pp \rightarrow \tilde{\chi}_2^0 \tilde{\chi}_2^0$ in the $M_2 - \mu$ plane for $\sqrt{s} = 8$ TeV, where we take $\tan \beta = 45$ and fix $M_1 = \frac{5}{3} M_2 \tan^2 \theta_W$.

In Figs. 12 to 14, we show the dependence of the total LO, NLO cross sections and the K factors on the squark mass for each scenario at $\sqrt{s} = 8$ and 14 TeV. We vary the squark mass from 500 to 2000 GeV. Here, there arise the same dominant scenarios as ones in the center-of-mass energy dependence of the cross sections. The LO

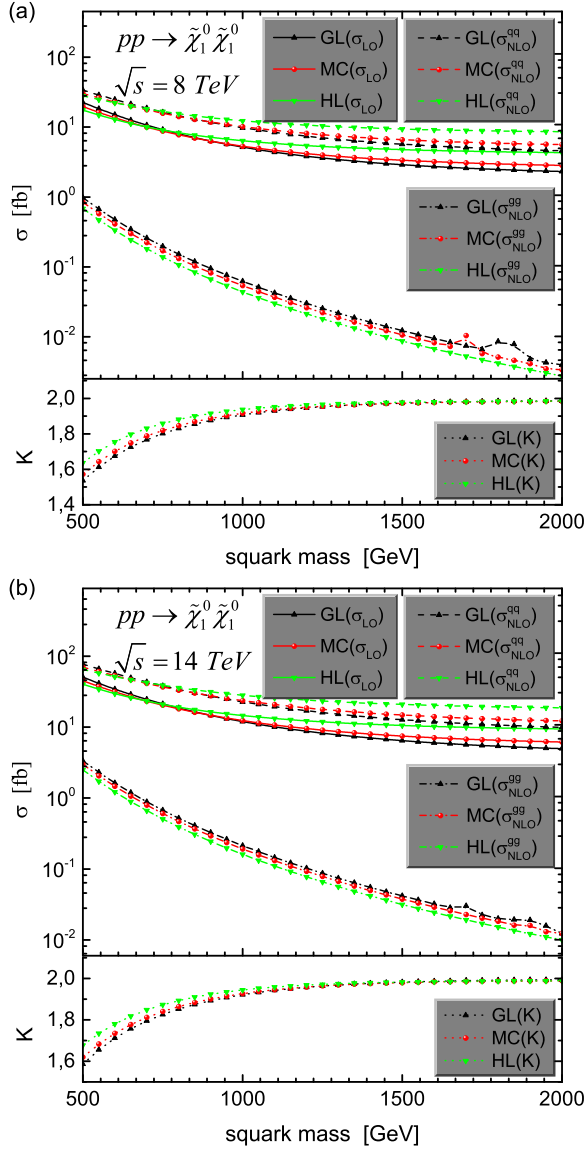


FIG. 12. (color online). Total LO and NLO cross sections for the process $pp \rightarrow \tilde{\chi}_1^0 \tilde{\chi}_1^0$ depending on the squark mass at (a) $\sqrt{s} = 8$ TeV and (b) 14 TeV. The lower panels show the K factor, $K = (\sigma_{NLO}^{qq} + \sigma_{NLO}^{gg})/\sigma_{LO}$.

and NLO cross sections for both $q\bar{q}$ annihilation and gg fusion are mainly determined by the squark mass. These decrease with the increment of the squark mass from 500 to 2000 GeV. When the squark mass grows by a factor of 4, the NLO cross sections are reduced by around one and two orders of magnitude for $q\bar{q}$ annihilation and gg fusion, respectively. We can see that the K factor

is sensitive according to increment of the squark mass. When the squark mass runs from 500 to 2000 GeV at

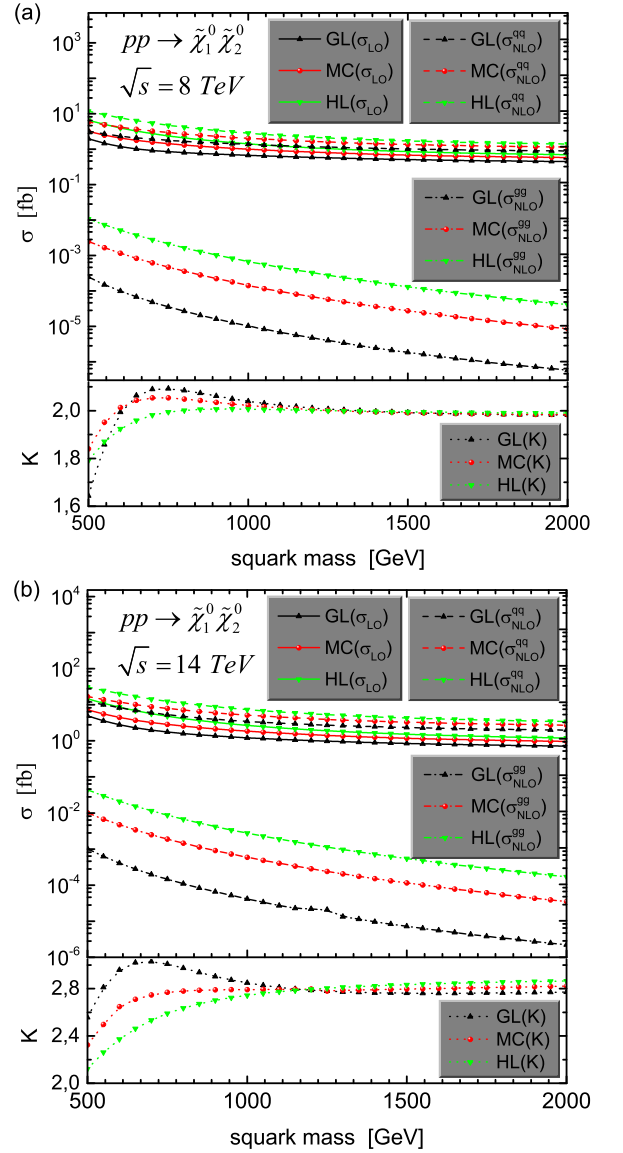


FIG. 13. (color online). Total LO and NLO cross sections for the process $pp \rightarrow \tilde{\chi}_1^0 \tilde{\chi}_2^0$ depending on the squark mass at (a) $\sqrt{s} = 8$ TeV and (b) 14 TeV. The lower panels show the K factor, $K = (\sigma_{NLO}^{qq} + \sigma_{NLO}^{gg})/\sigma_{LO}$.

center-of-mass energy 8 TeV (14 TeV), the K factor increases from 1.54 to 1.99 (1.59 to 1.99) in the gauginolike scenario, from 1.57 to 1.98 (1.62 to 1.99) in the mixture-case scenario, and from 1.64 to 1.98 (1.68 to 1.99) in the Higgsino-like scenario for the process $pp \rightarrow \tilde{\chi}_1^0 \tilde{\chi}_1^0$ as shown in Figs. 12(a)-12(b). Furthermore, the K factor for the process $pp \rightarrow \tilde{\chi}_1^0 \tilde{\chi}_2^0$ increases from 1.64 to 1.98 (2.56 to 2.77) in the gauginolike scenario, from 1.84 to 1.98 (2.32 to 2.82) in the mixture-case scenario, and from 1.79 to 1.99 (2.12 to 2.87) in the Higgsino-like scenario for center-of-mass energy 8 TeV (14 TeV) as shown in

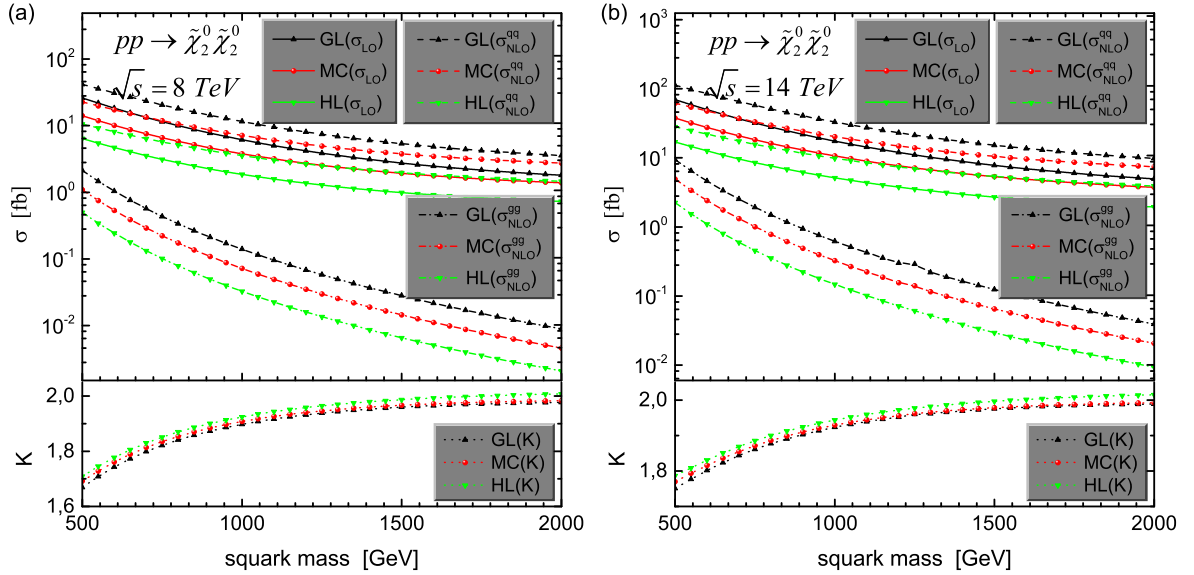


FIG. 14. (color online). Total LO and NLO cross sections for the process $pp \rightarrow \tilde{\chi}_2^0 \tilde{\chi}_2^0$ depending on the squark mass at (a) $\sqrt{s} = 8$ TeV and (b) 14 TeV. The lower panels show the K factor, $K = (\sigma_{NLO}^{qq} + \sigma_{NLO}^{gg})/\sigma_{LO}$.

TABLE III. Total LO, NLO cross sections (in fb) and corresponding K factors as a function of the squark mass at center-of-mass energy $\sqrt{s} = 8$ and 14 TeV for each scenario. Here the K factor is $K = (\sigma_{NLO}^{qq} + \sigma_{NLO}^{gg})/\sigma_{LO}$.

	\sqrt{s} (TeV)	$m_{\tilde{q}}$ (TeV)	$pp \rightarrow \tilde{\chi}_1^0 \tilde{\chi}_1^0$				$pp \rightarrow \tilde{\chi}_1^0 \tilde{\chi}_2^0$				$pp \rightarrow \tilde{\chi}_2^0 \tilde{\chi}_2^0$			
			σ_{LO}	σ_{NLO}^{qq}	σ_{NLO}^{gg}	K	σ_{LO}	σ_{NLO}^{qq}	σ_{NLO}^{gg}	K	σ_{LO}	σ_{NLO}^{qq}	σ_{NLO}^{gg}	K
HL	8	1	6.37	12.30	0.044	1.94	1.40	2.82	$6.7 \cdot 10^{-4}$	2.01	1.85	3.53	0.033	1.92
		2	4.32	8.57	0.003	1.98	0.70	1.39	$4.1 \cdot 10^{-5}$	1.99	0.73	1.46	0.002	2.01
	14	1	14.55	28.13	0.16	1.94	2.68	7.35	$2.8 \cdot 10^{-3}$	2.74	5.13	9.82	0.15	1.94
		2	9.41	18.71	0.001	1.99	1.20	3.43	$1.7 \cdot 10^{-4}$	2.87	1.95	3.91	0.009	2.01
GL	8	1	5.17	9.79	0.062	1.91	0.67	1.37	$1.0 \cdot 10^{-5}$	2.04	6.15	11.54	0.14	1.90
		2	2.31	4.59	0.004	1.99	0.45	0.88	$5.7 \cdot 10^{-7}$	1.98	1.81	3.57	0.009	1.98
	14	1	11.94	22.73	0.21	1.92	1.21	3.46	$4.1 \cdot 10^{-5}$	2.85	17.47	32.98	0.62	1.92
		2	4.97	9.90	0.012	1.99	0.72	1.99	$2.2 \cdot 10^{-6}$	2.77	4.95	9.81	0.039	1.99
MC	8	1	5.33	10.16	0.054	1.92	1.00	2.02	$1.4 \cdot 10^{-4}$	2.02	3.78	7.15	0.072	1.91
		2	2.83	5.61	0.003	1.98	0.58	1.14	$8.5 \cdot 10^{-6}$	1.98	1.39	2.75	0.005	1.98
	14	1	12.35	23.62	0.19	1.93	1.85	5.18	$5.9 \cdot 10^{-4}$	2.79	10.64	20.21	0.32	1.93
		2	6.15	12.23	0.012	1.99	0.97	2.73	$3.5 \cdot 10^{-5}$	2.82	3.74	7.43	0.021	1.99

Figs. 13(a)-13(b). Finally, the K factor for the process $pp \rightarrow \tilde{\chi}_2^0 \tilde{\chi}_2^0$ increases from 1.67 to 1.98 (1.75 to 1.99) in the gauginolike scenario, from 1.69 to 1.98 (1.77 to 1.99) in the mixture-case scenario, and from 1.71 to 2.01 (1.79 to 2.01) in the Higgsino-like scenario at center-of-mass energy 8 TeV (14 TeV) as illustrated in Figs. 14(a)-14(b). With a view to make easy precise comparisons with the experimental results, we list in Table III the numerical results of the LO, NLO cross sections and K factors for the squark mass 1 and 2 TeV at $\sqrt{s} = 8$ and 14 TeV. The results show that the NLO corrections increase the corresponding LO cross sections when squark mass varies from 500 to 2000 GeV.

Finally, the total LO, NLO cross sections and the K factors for the process $pp \rightarrow \tilde{\chi}_i^0 \tilde{\chi}_j^0$ versus the factoriza-

tion and renormalization scale μ_0 in the range from 100 to 1000 GeV at $\sqrt{s} = 8$ TeV are depicted in Figs. 15 through 17. These figures demonstrate the same dominant scenarios as ones in the dependence of the cross sections on the center-of-mass energy. From these figures we can also see that both LO and one-loop cross sections decrease slightly when the scale μ_0 goes up from 100 to 1000 GeV for each scenario. One can remark that the LO cross sections are nearly independent of the scale μ_0 . That is since the neutralino pair production process at Born-level contains only pure electroweak channels where there is not the renormalization scale dependence at the this level, and the energy scale dependence is only due to the PDFs being connected to the factorization scale. The corresponding K factors, on the other hand, decrease by

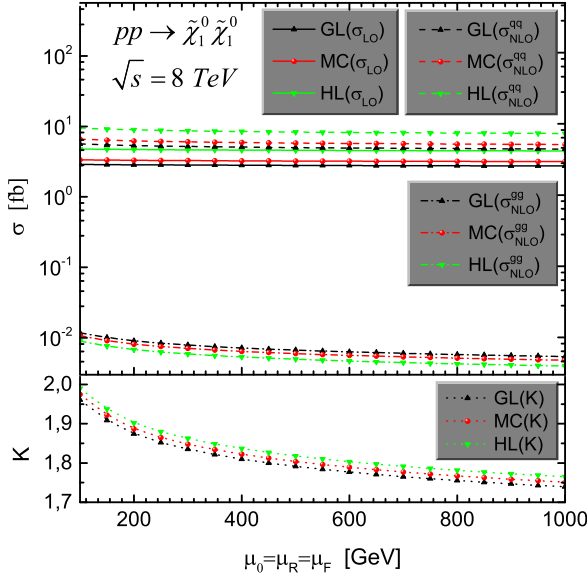


FIG. 15. (color online). Total LO and NLO cross sections depending on the renormalization and factorization scales for $pp \rightarrow \tilde{\chi}_1^0 \tilde{\chi}_1^0$ at $\sqrt{s} = 8$ TeV. The lower panel shows the K factor, $K = (\sigma_{NLO}^{qq} + \sigma_{NLO}^{gg})/\sigma_{LO}$.

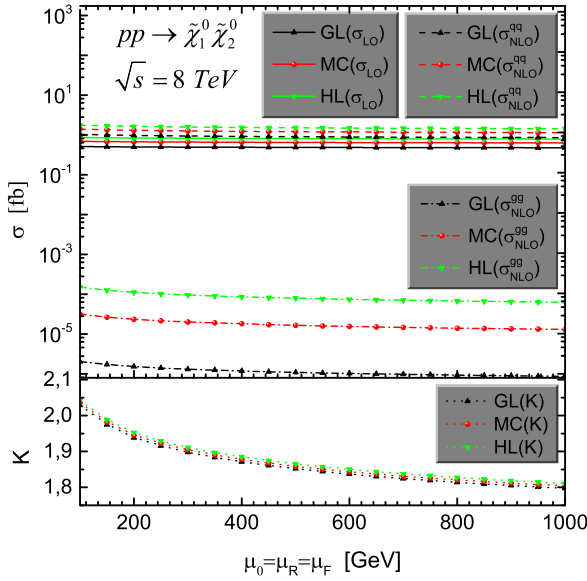


FIG. 16. (color online). Total LO and NLO cross sections depending on the renormalization and factorization scales for $pp \rightarrow \tilde{\chi}_1^0 \tilde{\chi}_2^0$ at $\sqrt{s} = 8$ TeV. The lower panel shows the K factor, $K = (\sigma_{NLO}^{qq} + \sigma_{NLO}^{gg})/\sigma_{LO}$.

about 11 percent when the scale μ_0 varies from 100 to 1000 GeV for each scenario. Figure 15 shows that the K factor for $pp \rightarrow \tilde{\chi}_1^0 \tilde{\chi}_1^0$ decreases from 1.99 to 1.76, 1.96 to 1.74, and 1.97 to 1.75 in the Higgsino-like scenario, gaugino-like scenario, and mixture-case scenario when increasing the scale μ_0 from 100 to 1000 GeV, respectively. Fig-

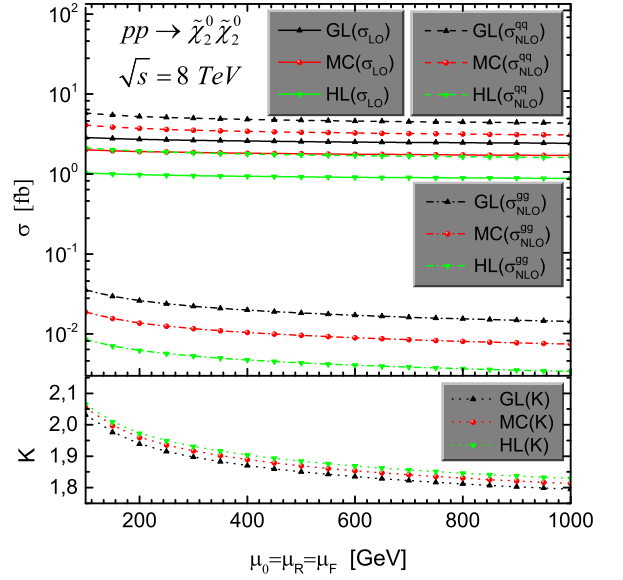


FIG. 17. (color online). Total LO and NLO cross sections depending on the renormalization and factorization scales for $pp \rightarrow \tilde{\chi}_2^0 \tilde{\chi}_2^0$ at $\sqrt{s} = 8$ TeV. The lower panel shows the K factor, $K = (\sigma_{NLO}^{qq} + \sigma_{NLO}^{gg})/\sigma_{LO}$.

ure 16 shows that the K factor for $pp \rightarrow \tilde{\chi}_1^0 \tilde{\chi}_2^0$ decreases from 2.04 to 1.81, 2.03 to 1.80, and 2.04 to 1.80 in the Higgsino-like scenario, gaugino-like scenario, and mixture-case scenario when increasing the scale μ_0 from 100 to 1000 GeV, respectively. Figure 17 displays that the K factor for $pp \rightarrow \tilde{\chi}_2^0 \tilde{\chi}_2^0$ decreases from 2.06 to 1.83, 2.03 to 1.79, and 2.05 to 1.81 in the Higgsino-like scenario, gaugino-like scenario, and mixture-case scenario when increasing the scale μ_0 from 100 to 1000 GeV, respectively. These results show that the K factors are mostly sensitive to the scale μ_0 .

It should be noted that analysis of our calculations is not directly dependent on the mass of the Higgs. The K factor is not sensitive to the mass of the Higgs. We have a figure with full spectrum. However, we also have alternative scenarios and have compared them with the CMSSM benchmark point. As is seen in the figures, the cross sections calculated in the alternative scenarios are more dominant according to the CMSSM 40.2.4 benchmark point.

We can see that one-loop contributions are positive and essentially increase the LO cross sections. Additionally, the curves in the figures display that the one-loop cross sections for gg fusion have a larger incline than the $q\bar{q}$ annihilation; the effect being primarily on account of the behavior of the gluon PDFs. It can be also seen that the one-loop cross sections for the $q\bar{q}$ annihilation always are larger than the LO cross sections, while one-loop cross sections for the gg fusion are less than these. However, note that the gg fusion contribution can be comparable to the $q\bar{q}$ one in the low $\tan\beta$ regime.

VI. CONCLUSION

In this work we have computed one-loop contributions for the neutralino pair production processes via quark-antiquark annihilation and gluon-gluon fusion in proton-proton collisions at the LHC. We have investigated numerically the effects of the center-of-mass energy, the M_2 - μ mass plane, the squark mass, the factorization and renormalization scales on the total Born, NLO cross sections and K factor for the CMSSM, and three different scenarios called the gauginolike, Higgsino-like, and mixture case.

The numerical results show that the NLO corrections increase the Born cross sections. The one-loop contributions of the process $q\bar{q}$ annihilation are significant for the experimental and phenomenological works in connection with the neutralino pair productions at the LHC and the future colliders. The K factor varies in the range from 1.96 to 2.00 when center-of-mass energy goes from 7 to 14 TeV. Our scenarios dominate over the CMSSM 40.2.4 benchmark scenario for each process. It is clear that the strong dependence of the cross sections and K factor on the parameters M_2 and μ is remarkable. From the discussed results in the M_2 - μ mass plane, we can

conclude that pure gaugino couplings dominate in the case $i = j$, whereas pure Higgsino couplings enhance in the case $i \neq j$ for $pp \rightarrow \tilde{\chi}_i^0 \tilde{\chi}_j^0$. In addition, the maximum values of the K factor are obtained in the region $\mu \lesssim 500$ GeV and $400 \lesssim M_2 \lesssim 1000$ GeV for processes $pp \rightarrow \tilde{\chi}_1^0 \tilde{\chi}_1^0$, $\mu \lesssim 500$ GeV and $M_2 \lesssim 500$ GeV for processes $pp \rightarrow \tilde{\chi}_1^0 \tilde{\chi}_2^0$, and $\mu > M_2$ for process $pp \rightarrow \tilde{\chi}_2^0 \tilde{\chi}_2^0$. The LO and NLO cross sections for both $q\bar{q}$ annihilation and gg fusion are considerably determined by the squark mass. When the squark mass increases by a factor of 4, the NLO cross section is pulled down by around one and two orders of magnitude for $q\bar{q}$ annihilation and gg fusion, respectively. However, the dependence of the LO cross section on the scale μ_0 shows that it is nearly independent of the scale μ_0 for the above-mentioned reasons. We can also see that the K factors decrease by about 11% as the increment of the scale μ_0 from 100 to 1000 GeV.

It should be underlined that there appear sizeable one-loop contributions to the neutralino production, which considerably increase the extracted bounds on the gaugino masses from the negative results for these particles at the LHC. In our opinion these results will be helpful for investigations and analysis of the different neutralino decay channels and for gaugino and Higgsino production in the LHC and future hadron colliders.

-
- [1] H. P. Nilles, *Phys. Rep.* **110**, 1 (1984).
 - [2] H. E. Haber and G. L. Kane, *Phys. Rep.* **117**, 75 (1985).
 - [3] H. Baer and X. Tata, *Weak Scale Supersymmetry: From Superfields to Scattering Events* (Cambridge University Press, Cambridge, England, 2006).
 - [4] P. Fayet, *Phys. Lett.* **69B**, 489 (1977); G. R. Farrar and P. Fayet, *Phys. Lett.* **76B**, 575 (1978).
 - [5] D. I. Kazakov, *Phys. Rep.* **344**, 309 (2001), arXiv:hep-ph/0001257.
 - [6] J. L. Feng, *Annu. Rev. Astron. Astrophys.* **48**, 495 (2010), arXiv:1003.0904 [astro-ph.CO].
 - [7] G. Jungman, M. Kamionkowski, and K. Griest, *Phys. Rep.* **267**, 195 (1996), arXiv:hep-ph/9506380.
 - [8] K. Griest and M. Kamionkowski, *Phys. Rep.* **333**, 167 (2000).
 - [9] S. Chatrchyan *et al.* (CMS Collaboration), *Phys. Lett. B* **716**, 30 (2012), arXiv:1207.7235 [hep-ex].
 - [10] G. Aad *et al.* (ATLAS Collaboration), *Phys. Lett. B* **716**, 1 (2012), arXiv:1207.7214 [hep-ex].
 - [11] ATLAS Collaboration, Report No. **ATLAS-CONF-2013-047** (2013).
 - [12] ATLAS Collaboration, Report No. **ATLAS-CONF-2013-062** (2013).
 - [13] CMS Collaboration, Report No. **CMS-PAS-SUS-13-012** (2013).
 - [14] K. L. Chan, U. Chattopadhyay, and P. Nath, *Phys. Rev. D* **58**, 096004 (1998), arXiv:hep-ph/9710473.
 - [15] For a recent review see, e.g. T. Han, S. Padhi, and S. Su, *Phys. Rev. D* **88**, 115010 (2013).
 - [16] J. Abdallah *et al.* (DELPHI Collaboration), *Eur. Phys. J. C* **31**, 421 (2003).
 - [17] J. Beringer *et al.* (Particle Data Group), *Phys. Rev. D* **86**, 010001 (2012).
 - [18] H. Baer, V. Barger, P. Huang, D. Mickelson, A. Mustafayev, W. Sreethawong, and X. Tata, *Phys. Rev. Lett.* **110**, 151801 (2013), arXiv:1302.5816 [hep-ph]; *J. High Energy Phys.* **12** (2013) 013.
 - [19] W. Beenakker, M. Klasen, M. Krämer, T. Plehn, M. Spira, and P. M. Zerwas, *Phys. Rev. Lett.* **83**, 3780 (1999); **100**, 029901(E) (2008), arXiv:hep-ph/9906298.
 - [20] J. Yi, M. Wen-Gan, H. Liang, Y. Zeng-Hui, and H. Pietschmann, *Phys. Rev. D* **62**, 035006 (2000), arXiv:hep-ph/0003291.
 - [21] A. I. Ahmadov, I. Boztosun, R. K. Muradov, A. Soylyu, and E. A. Dadashov, *Int. J. Mod. Phys. E* **15**, 1183 (2006).
 - [22] G. J. Gounaris, J. Layssac, P. I. Porfyriadis, and F. M. Renard, *Phys. Rev. D* **70**, 033011 (2004).
 - [23] G. Cullen, N. Greiner, and G. Heinrich, *Eur. Phys. J. C* **73**, 1 (2013).
 - [24] A. I. Ahmadov and M. Demirci, *Int. J. Mod. Phys. A* **28**, 1350077 (2013), arXiv:1307.3779 [hep-ph].
 - [25] F. del Aguila, A. Culatti, R. Munoz Tapia, and M. Perez-Victoria, *Nucl. Phys.* **B537**, 561 (1999).
 - [26] W. Siegel, *Phys. Lett.* **84B**, 193 (1979).
 - [27] D. Capper, D. Jones, and P. van Nieuwenhuizen, *Nucl. Phys.* **B167**, 479 (1980).
 - [28] D. Stöckinger, *J. High Energy Phys.* **03** (2005) 076, arXiv:hep-ph/0503129.
 - [29] A. I. Ahmadov and M. Demirci, *Phys. Rev. D* **88**, 015017 (2013), arXiv:1307.3777 [hep-ph].
 - [30] S. S. AbdusSalam *et al.*, *Eur. Phys. J. C* **71**, 1835 (2011),

- [arXiv:1109.3859 \[hep-ph\]](#).
- [31] A. H. Chamseddine, R. L. Arnowitt, and P. Nath, *Phys. Rev. Lett.* **49**, 970 (1982).
 - [32] R. L. Arnowitt and P. Nath, *Phys. Rev. Lett.* **69**, 725 (1992).
 - [33] G. L. Kane, C. Kolda, L. Roszkowski, and J. D. Wells, *Phys. Rev. D* **49**, 6173 (1994).
 - [34] B. C. Allanach, *Comput. Phys. Commun.* **143**, 305 (2002).
 - [35] J. Küblbeck, M. Böhm, and A. Denner, *Comput. Phys. Commun.* **60**, 165 (1990); T. Hahn, *Comput. Phys. Commun.* **140**, 418 (2001).
 - [36] T. Hahn and C. Schappacher, *Comput. Phys. Commun.* **143**, 54 (2002), [arXiv:hep-ph/0105349](#).
 - [37] T. Hahn and M. Perez-Victoria, *Comput. Phys. Commun.* **118**, 153 (1999), [arXiv:hep-ph/9807565](#).
 - [38] G. Passarino and M. J. G. Veltman, *Nucl. Phys.* **B160**, 151 (1979).
 - [39] S. Heinemeyer, W. Hollik, and G. Weiglein, *Comput. Phys. Commun.* **124**, 76 (2000), [arXiv:hep-ph/9812320](#).
 - [40] A. D. Martin, W. J. Stirling, R. S. Thorne, and G. Watt, *Eur. Phys. J. C* **63**, 189 (2009), [arXiv:0901.0002 \[hep-ph\]](#).
 - [41] M. R. Whalley, D. Bourilkov, and R. C. Group, The Les Houches Accord PDFs (LHAPDF) and Lhaglu, <http://hepforge.cedar.ac.uk/lhapdf>, [arXiv:hep-ph/0508110](#).